IMPLICATIONS OF SURFACE FINISH AND SUB-SURFACE POROSITY ON COMPONENT LIFE PREDICTION

Alison J. McMillan[1], Rhys Jones[2]

[1]Faculty of Arts, Sciences and Technology, Wrexham Glyndwr University, Mold Road, Wrexham, LL11 2AW, UK.

[2]Centre of Expertise Structural Mechanics, Department of Mechanical and Aerospace Engineering, Monash University, Clayton, VIC 3800, Australia.

Corresponding Author:

Alison McMillan, ajmcmillan17@gmail.com , +44 777 329 7834

Orcid Numbers:

Alison McMillan 0000-0003-4191-096X

Rhys Jones 0000-0003-3197-2796

ABSTRACT

High duty engineering component life is usually demonstrated through extensive testing and statistical analysis applied to empirical curve-fit equations. Because of this, the extent of the testing required is huge and costly: it must consider the load cycle range and test to high numbers of cycles. Furthermore, this testing must be repeated for every material, method of manufacture, and subsequent post-processing. Additive Manufacturing (AM) for high duty components has brought to the fore the question of the effect of porosity and surface roughness on fatigue life. Because there is relatively little service life experience, it is possible that the testing approach could also fail to represent conservatively the true life of a critical component. The authors propose the development of a fatigue model based on well-established engineering physics principles, by creating computational specimens with modelled surface roughness and porosity, and subjected to cyclic loading using Finite Element Analysis. They show that the combination of roughness features and sub-surface pores leads to an equivalent plastic strain distribution pattern that suggests an emergent physical process. Such a phenomenological understanding of the fatigue failure process should lead to improved life prediction techniques, more cost effective test procedures, and the development of better AM methods.

Keywords: additive manufacturing, fatigue, FEA, porosity, residual stress, surface roughness

Acknowledgements:

1. INTRODUCTION

The overarching motivation of the work reported in this paper is to improve fatigue life prediction for aerospace components. Traditionally, fatigue assessment is heavily dependent on testing and statistical analysis. With the introduction of new materials and methods of manufacture, such as composites and Additive Manufacturing, the material property and component geometry variation places significantly greater demands on the numbers of tests required to obtain satisfactory statistical confidence in the test results. In the engineering sector, there is an increasing trend to reduce testing, and thus testing costs, by relying more on validated computational modelling. In the context of fatigue assessment, this presents a problem, because fatigue understanding is largely based on experimental results and empirical models, such as the NASGRO crack growth equation. Empirical models can be used in a computational context, but still require compelling data evidence to validate their applicability.

A more desirable objective is to create a modelling capability that is based on well-established physical principles, and to link the fatigue assessment to measurable attributes of the material properties and component geometry. That is the objective for this present paper, which is entirely based on computational modelling. Two types of component geometry feature are modelled: surface roughness and porosity. The material is modelled as a simple piece-wise linear elastoplastic material, and the computational specimen geometries are subjected to cyclic loading, at load levels that would be below the yield threshold for specimen without roughness or porosity. We assess the results of these computations, and compare with the empirical and pragmatic methods of fatigue assessment. Although it is difficult to arrive at a firm conclusion at this stage, we believe that the computational models presented here enhance our understanding and could form part of a future fatigue assessment methodology. The reader might be critical of the simplifications and approximations we have made, but, as Einstein is frequently paraphrased as saying, “Everything should be kept as simple as possible, but not simpler” – a paraphrasing of Occam’s Razor. The investigation of further model enhancement and complexity will be the subject of future work.

The structure of this paper is as follows. In the present section, we provide the context and motivation for this work. In Section 2, we review existing understanding and the prior work on which the present work is predicated. In Section 3 we discuss the methodology which underpins this present work, using probing questions, based on Bacon’s [1] inductive principles. Section 4 explains the construction of the computational models used. Section 5 presents qualitative results to illustrate the interactive effects of surface roughness and subsurface porosity to create a pattern of stress and equivalent plastic strain (PEEQ) in the subsurface layer. In Section 6, we analyse this data and present results in answer to the probing questions set out in Section 3. Section 7 provides a detailed discussion of the methodology, the modelling methods used, the results obtained and weaknesses in our approach that could be addressed in future work, and proposes a potential route map for an analytical approach to fatigue life assessment for Additive Manufactured aerospace components. The conclusions to this paper are set out in Section 8.

2. REVIEW

2.1 Additive Manufacturing

Additive Manufacturing (AM) has become increasingly recognised as an important alternative method of manufacture, particularly for highly customised parts or parts with complex geometries [2]. The drivers for these first applications are practical issues, such as manufacturing flexibility, reduction in tooling costs, or better utilisation of material and

sustainability [3]. As AM has become a more mature capability, more challenging applications are coming into consideration, such as components for aerospace or space vehicles, and with this, greater concern for the materials properties of the as-manufactured component [4]. The drivers for such applications include the environmental and material cost requirement to reduce the *"buy-to-fly"* ratio for expensive aerospace alloys, or to manufacture lightweight components with an internal hollow structure that are impossible to make any other way. Another emerging and important driver is the ability to manufacture parts in the field or at remote locations.

A more significant issue for AM for critical load bearing component applications is to know the mechanical performance of additively manufactured material. For the United States Air Force (USAF), the prediction of the Durability and Damage Tolerance (DADT) of a metallic part is based on linear-elastic fracture mechanics (LEFM) principles [5, 6]. This analysis process makes extensive use of what is termed the *"equivalent initial damage size (EIDS)"*, which represents the size of the damage that must be assumed to exist when the aircraft enters service. The size of the EIDS required for AM aerospace parts is discussed in [6].

It is well-known that surface finish has an influence on the fatigue performance of a test specimen, and so it is natural that the surface roughness of an as-manufactured AM component has received a great deal of interest from researchers looking to extend AM as a method of manufacturing aerospace parts [8, 9, 10, 11, 12, 12], for example, [8] stated:

"The surface roughness is the single most severe factor for fatigue for additive manufactured materials".

The purpose of this current paper is to argue that surface roughness is not the only critical consideration, and to demonstrate that considering both surface roughness and sub-surface porosity can reveal more detail about the mechanism and development of damage accumulation in the material over multiple loading cycles. The published literature contains some indications of the significance of considering both surface roughness and sub-surface porosity together, rather than as two separate phenomena, but in general it does not seem to be generally recognised. For example, Masuo *et al* [13] investigated defects, surface roughness and HIPping of Titanium alloy AM. They describe two types of pores: gas pores and lack of fusion (LOF). They state, "Many defects which were formed at subsurface were eliminated by HIP and eventually HIP improved fatigue strength drastically…", and note that surface polishing and HIPping substantially improve fatigue properties. On closer inspection of their stress-life (S-N) graphs it can be clearly seen that surface machining alone has a greater improvement than HIPping alone, but when both operations were performed the improvement was greater than might be assumed from summing the improvements from the two individual effects. In another example, Chan and Peralta-Duran [14] consider fatigue in AM parts, and use an analytical model to treat surface notches as fatigue crack nucleation sites. Their measured fatigue life results for as-built AM parts do not seem to follow the trend lines of their predictions, whereas the equivalent results for surface machined AM parts do. This seems to suggest that, in neglecting the combined surface morphology effects of neighbouring notches and sub-surface porosity, an important physical aspect is missing from their model.

It is hoped that the present computationally based study can help to identify the significant physical aspects that must be taken into account. Ideally, it would be desirable to be able to in link physical surface morphology feature measurements directly to the EIDS value used to certify AM parts for aerospace applications.

2.2 Fatigue life testing, statistics and approaches for aircraft certification

However good a model is, the physical experiment is generally preferred because there may be parameters or effects within the real test specimen that are not measured or appreciated in

the analysis but have a significant effect on the result obtained. Fatigue life prediction has always been built on test data and statistical analysis with the test specimens made from the same material and fabricated using the same manufacturing processes as the engineering component for which the fatigue life prediction is required. The practical attractions of Additive Manufacturing have to be tempered with the crucial requirement that the predicted operational life must be conservative. Since certification requires a damage tolerance/durability analysis [5, 6], there have been many test programmes from which the crack growth rate versus the stress intensity range during a load cycle curves, da/dN versus ΔK, have been generated for a range of metal alloys, and different Additive Manufacturing processes as well as for conventionally manufactured aerospace materials [15-22]. A review of the *"state of the art"* of the damage tolerant and durability analysis methodologies needed for aerospace applications is given in [22]. In this context [23-27] have shown that the Hartman-Schijve variant of the NASGRO crack growth equation can be used to represent crack growth in AM materials accurately as well as crack growth in parts repaired using additive metal deposition. The fact that the same formulation works so well for such a wide range of materials and manufacturing processes suggests that a phenomenologically based predictive understanding of fatigue life could be within grasp.

Regardless of which crack growth equation is used in the DTDA design/assessment of an AM part, or an AM repair to an existing part, the choice of the EIDS is a key factor in determining the operational life of the part. Here it is important to note that, as stated in the certification standard MIL-STD-1530D [5], the role of testing is merely to *"validate or correct analysis methods and results"*. This raises the question can we relate EIDS to a physical quantity?

As previously noted the certification requirements for AM components in military aircraft are enunciated in the recently published EZ-SB-19-01 [6], which is in-turn based on MIL-STD-1530D [5]. Prior to the introduction of EZ-SB-19-01, Structures Bulletin EZ-SB-13-001 [28] stated that AM is *"NOT RECOMMENDED without extensive testing and AFRL/RX* [Air Force Research Laboratory, Materials and Manufacturing Directorate] *support"*. Thus, while not recommended, the use of AM was not entirely ruled out. MIL-STD-1530D set out the evaluation requirements of *(i) "Stability"* (here this refers to process stability), *(ii) "Producibility"* (the need to reproduce the same capabilities at volume production rates), *(iii) "Characterization of* […] *properties"*, *(iv) "Predictability of structural performance"*, and *(v) "Supportability"* (product sustainment throughout the lifecycle).

The 2019 EZ-SB-19-01 [6] directive builds on these requirements, and discusses a range of aspects or features that might contribute or act as *"surrogate damage"*. To this end EZ-SB-19-01 cites *"four attributes of surrogate damage: damage type, damage size, damage orientation, and damage location"*. Thus, both surface roughness and defect size are considered together, and (to some extent) in the same way. It further discusses the damage tolerance approach and the requirement for an *"Equivalent Initial Damage Size (EIDS)"*. Here EIDS is defined as per MIL-STD-1530D [5], *viz.*:

"an analytical characterization of the initial quality of the aircraft structure at the time of manufacture, modification or repair. The EIDS distribution is derived by analytically determining the initial damage size distribution that characterizes the measured damage size distribution observed during test or in service."

Given that the operational life of the structure is determined by analysis, this means that the EIDS is determined by the size of the initial flaw that will yield the measured test life. As explained by Lincoln [29], when the USAF adopted damage tolerance, they made the decision to separate the process for assessing safety from the process for assessing aircraft durability. Consequently, as shown in [29], EIDS can be a function of the da/dN versus ΔK curve used in the analysis. Furthermore, Lincoln also revealed that for a durability analysis it is necessary to use the da/dN versus ΔK curve corresponding to the growth of small

naturally occurring cracks. This is explained in more detail in [16]. If this is not done then the EIDS values are a function of the test spectra [29]. On the other hand, if the small crack da/dN versus ΔK curve is used in the DTDA analysis, then the EIDS is closely related to the actual size of the material discontinuities from which the cracks grow [16-17, 25-27, 29-32].
EZ-SB-19-01 notes that for AM parts surface roughness is a key physical property; however, surface roughness is strongly dependent on the AM process, and the choice of definition for roughness [33-36], with surface roughness sizes that can lie in the range of 10s to 100s of μm. In this context, the use of the fractal box dimension to characterize surface roughness is particularly appealing given its success in characterising crack growth [37-41], its ability to characterize the failure surfaces associated with additive metal deposition [40], and its role in the development of the Boeing Bogel surface treatment [42].
With regard to flaws such as defects, inclusions, porosity pores and surface breaking features, these are also typically in the size range 10s to 100s of μm. Finfrock et al. [43] describe the occurrence of porosity for parts made using Selective Laser Melting (SLM), highlighting the value of the HIPping process and the quality of the feedstock powder. Figure 1 illustrates the situation of porosity occurring close to the surface: the pore illustrated is roughly 50 μm across and centred at about 100 μm below the nominal surface. In another study by Du Plessis et al [44], using X-ray micro CT to examine AM Titanium alloy material subjected to HIPping, clusters of < 70 μm pores at a sub-surface depth of about 300 μm are illustrated. The authors explain, by analogy to similar observations made of cast components, that sub-surface pores that are connected to the surface by micro-cracks cannot be eliminated by HIPping. Tammas-Williams *et al* [45] and Léonard *et al* [46] also use X-ray CT to investigate defect location and type in Titanium alloy samples made using the SLM. Tammas-Williams *et al* state that the "majority of pores" are "spherical and relatively small (< 75 μm)" and that "only ~ 3% of pores" have an aspect ratio of greater than 1.5. In another interesting paper by Guo et al [47] laser shock peening of AM Titanium alloy is investigated. The paper illustrates a sub-surface pore of nearly circular form, with a diameter of approximately 5 μm, and situated about 30 μm beneath the surface. For further examples, Kruth et al [48] review a huge variety of AM process.
Finally, it should be noted that EZ-SB-19-01 [6] requires a minimal EIDS of 0.01 inches (0.254 mm), and that Airbus have stated that, for AM parts, an EIDS of greater than 0.5 mm is rarely seen [49]. This latter statement is important given the statement in EZ-SB-19-01 that for the damage size for durability crack growth analysis shall be based on a probability of exceeding the EIDS of $1x10^{-3}$.

2.3 Representative modelling approaches

There are two main areas of work on which this present work is based. Firstly, there is the body of work concerned with computational modelling of heterogeneous materials, in order to model their properties. The second area is concerned with the modelling of surface texture. In both cases, it is assumed that there would be a full computational analysis of the modelled geometry, probably using Finite Element Analysis (FEA), and probably including some non-linear elastic or elastoplastic material properties, to determine stresses and plastic strains. An interesting proxy approach is proposed [50] whereby the strain field can be related to a geodesic property, which might provide a faster but more approximate method for assessing such models.

2.3.1 Modelling of heterogeneous materials

The work in this area is very wide ranging, and includes heterogeneity in many forms, from the random patterns of metal crystal grain structure, porosity and modelling of

foams, through to the regular structure of a perfect composite material. Authors typically model a Representative Volume Element (RVE) of material, applying boundary conditions based on symmetry conditions [50-55]. Where the objective is to understand bulk material properties based on a detailed local model, this is a sensible approach: consider a notional pair of neighbouring RVEs. Both would be undergoing similar levels of loading and deforming in a similar way. The boundary between them would transfer little overall stress or strain when averaged over its length.

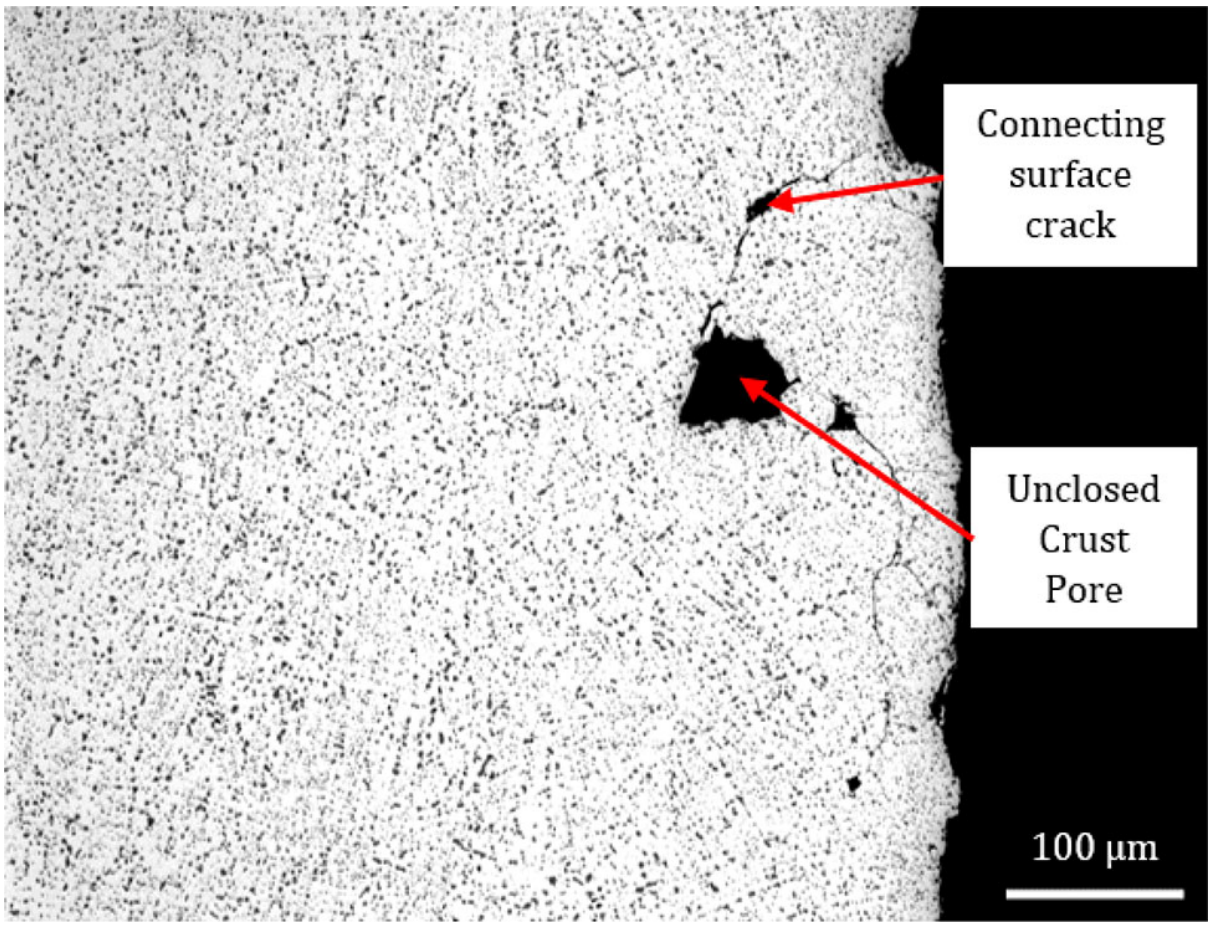

Figure 1. Example of sub-surface porosity.
Reprinted by permission from Springer, *Metallograpgy, Microstructure, and Analysis*, "Effect of Hot Isostatic Pressing and Powder Feedstock on Porosity, Microstructure, and Mechanical Properties of Selective Laser Melted AlSi10Mg" CB Finfrock, A Exil, JD Carroll, L Deibler (2018) [43].

For the modelling of bulk material with very randomly varying internal structure, reliance on the RVE approach can be misleading. By defining a particular RVE, then the internal heterogeneous material structure of that RVE is defined, and then, as a result of the boundary condition symmetry assumptions, it is replicated across the infinite material domain. Thus the model is one of a patterned structure and not a random one. The same is also true for the case of a mixed dimensional problem, one concerned with bulk properties and also surface features or lead crack propagation, the assumptions made for boundary conditions in RVE modelling no longer apply. The reason for this becomes obvious if one again considers the two neighbouring

notional RVEs: one is comprised only of bulk material, but the other includes a free surface. It is now clear that the assumption of similar levels of loading and deformation in these two RVEs is inappropriate, and so to make any assumption about stress-strain transfer at the boundary would be erroneous. In such a case, it is necessary to make a much larger domain model, and pad the boundaries with excess material, so that the areas of interest within the model are a long way away from the influence of any inappropriate boundary condition [56-58].

2.3.2 Surface roughness and surface effect representation

It is well-known that in fatigue coupon testing, the quality of the surface finish has a significant effect on the fatigue life achieved [33-34]. In classical stress analysis, it is well-known that surface notches create stress concentrations or raisers, and solutions for many particular geometrical shapes have been tabulated [59]. More recently, it has been suggested that surface roughness can be assessed using the same approach used for short cracks [60].

In order to replicate these observations in a model, it is necessary to have a means to characterise the surface texture of a typical engineering component [61]. Other authors have measured surface texture directly using a variety of methods, the highest precision method currently being Atomic Force Microscopy [62]. A recent review of surface texture of additively manufactured materials has been reported by Townsend *et al.* [35], providing many images of many surface textures pre- and post-finishing processing. Another recent report, by Triantaphyllou *et al.*, [36] focusses on metrology methods and provides some contrasting information. It is believed that surface roughness can be considered to be fractal, with similar geometric features appearing at different length-scales, and this is certainly a useful starting point for generating models of surface roughness [63-64]. Thus, although it is recognised that surface roughness is particularly significant, it is not entirely clear how fractal, or sub-surface phenomenology, such as surface braking cracks or porosity, should be included.

2.3.3 Material grain structure and methods of manufacture

It is reasonable to consider that the final surface texture of an engineering component might be significantly influenced by the particular material in question, the materials processing, the method of manufacture, any finishing techniques applied, and also any environmental effects to which it might have been subjected. This very rapidly leads an unwieldly set of parameters, each of which might have a relatively greater or lesser influence on the actual surface texture.

In conventional metallic component manufacturing, the materials processing leads to the development of a particular crystal grain structure. It is well-known that particular materials with particular grain structures have better fatigue performance than others that are chemically similar but structurally different [34]. There is also a consequence to the surface texture: the nature and typical size of the grain structure will have an effect on the particular surface finish that is obtained following subtractive processes such as machining, grinding or polishing. Thus, it is easy to see how the connection between fatigue performance and surface finish can become conflated with fatigue performance and grain structure. As a result, there are a number of authors developing detailed FEA models of crystal grain structure, but without including surface texture modelling [53-55]. The results of these analyses are qualitatively

interesting and suggest phenomenological processes in the development of failure, but perhaps show only a part of the overall picture.
In Additive Manufacturing (AM), the process is quite different to the conventional processes, and it is recognised [65] that AM processes produce microstructures that are different from those of conventionally manufactured materials. There are many different forms of AM, so it might be expected that the material produced would be quite different; however, it does seem from the consistency in the test evidence [5-12, 15-22, 66] that there is an implicit connection between microstructure and surface texture. Therefore, differences might be accounted for by parameter choice, rather than being due to significant differences in physics.

2.3.4 Surface geometry representation in fatigue modelling

Conventional fatigue theory is often based on the assumption of an initial crack, like EIDS. Gorelik suggests that the surface geometry can stand in place of the initial crack [60], but, as discussed above, it is still not clear quite what surface measurement would provide the associated EIDS. Describing a surface or a crack surface as *"fractal"* implies a non-integral dimension: something between a surface and a volume. The immediate sub-surface of a piece of material may contain flaws, porosity, and perhaps immediate sub-surface cracks. Considering the latter, before the surface is broken, these would be sub-surface phenomena, but as soon as the crack breaks the surface, the entire crack becomes part of the surface. Physically, these two situations are similar, so it seems that our understanding and representation of *"surface geometry"* might need to include the phenomenology of the immediate sub-surface porosity.
It has also been suggested [67] that, for the damage tolerant design of an AM part, the use of an EIDS of 1.27 mm is sufficiently large that the effect of surface roughness and near surface porosity can be ignored.
In the description here, we follow the ASTM E647-13a [68] definitions of *"small"* and *"long"* cracks. For small naturally occurring cracks, the influence of the microstructural size on crack growth has been found to be minimal [15]. For long cracks, the grain size can influence the crack growth rate significantly; however, since the focus in the present paper is on the surface geometry representation, and since, for small cracks, the effect of grain size is generally small [15], this suggests that modelling individual grains within the sub-surface would be unnecessary, at least in the first instance.

3. METHODOLOGY

The basis of the methodology to be applied here is as follows. It is first necessary to reflect on the tools or models that are reasonably available to use. The tools are *(i)* the Abaqus Finite Element Analysis (FEA) software package [69], and *(ii)* geometry creation and statistical analysis tools available through Python scripting [70]. Following prior representative modelling approaches (Section 2.3) reviewed above, it has been established that 2D computational specimen geometry with surface roughness and circular void porosity can be generated randomly based on generating algorithms (heuristic tools), and that these geometries can be adequately meshed and characterised. Thus, it is reasonable to expect that fair computational specimens can be created, and repeatable and statistically reliable results can be obtained from them. Any comparison of results would require assessment of the statistical variation of the "porosity volume fraction" in geometries created by the heuristic tool, and relate the geometries of the sets of results to the statistical distribution. The reader

may wish to skip ahead to Section 4 to learn about the modelling methods and how this requirement can be satisfied, before returning to this present section for more detailed scrutiny.

Second, we pose some probing questions, listing all the possible effects, and then reasoning as to an appropriate approach for testing the strength and significance of the effect. This is Bacon's "inductive reasoning" approach [1]. Using the tools and models to answer these questions through a series of computational experiments should then provide new science understanding.

The questions are:

1. **Effect of random variation** – What is the nature of differences in results for models with pores created by the same heuristic tool, but with different random number seeding?
2. **Effect of length scale** – What is the significance of the relative size of pores and the roughness features of the surface profile?
3. **Effect of pore size and position** – What is the significance of the relative size of pores and the depth of the sub-surface region in which they appear?
4. **Effect of porosity volume fraction** – What is the significance of the porosity volume fraction and how can that be characterised?
5. **Effect of porosity distribution** – What is the significance of the porosity distribution and how can that be characterised?
6. **Effect of limiting scale** – Should the modelling reflect the limiting scale of continuum mechanics: should a molecular dynamics approach be applied?

A number of further questions will occur readily to the critical reader, but such questions would probably address issues with the design of the computational experiments, rather than the scientific outputs themselves. A discussion of the modelling methods is given in Section 7.

3.1 Effect of random variation

The first probing question actually conceals another: there is the question of the variability in the surface profile as well as in the placing of the pores. To some extent that concealed question is already answered in that the construction of the surface shows variation along its length, so the effect of different features and the interaction between those features can be observed, (see later, for example in Figure 5). The other part of the question concerns the relative placement of the pores on the domain, and the variability of that includes the variability of juxtaposition of pores with particular surface profile features. In this way, these two questions resolve down to one computational experiment.

> **Resolution 1**: for each computational analysis for a given set of input data, repeat the model building using a heuristic tool, so as to produce a number of sets of results from a corresponding number of similar models. To ensure that each similar model has a correspondingly similar porosity volume fraction, the heuristic tool must generate an even distribution of porosity.

3.2 Effect of length scale

The question of length scale applies to each combination of feature size employed in the modelling. The length scale dependent features defined in the present modelling scheme are: the surface profile, the maximum pore diameter, and the position and dimensions of the defined zone area.

The surface roughness profile combines aspects of several length scales. In defining that profile, the intention was to build in a fractal-like property. Because of FEA model size

limitations it is impractical to define roughness below a particular size. On the other hand, it is reasonable to consider roughness feature sizes to be similar to porosity feature sizes, so our concern is only with the relative sizes of both to within about an order of magnitude. Because the surface profile already has a fractal-like property spanning about an order of magnitude, this length scale issue is already addressed in the existing modelling approach.

Next, let us first consider the defined zone area. The defined zone height should not have a length scale effect, since it is set to be the same as the surface roughness band, and plays the same role: it enables greater variation within a model. In practice, the size of the defined zone height would play a statistical role, but this is not a question of the nature of the result to be achieved but of the precision of that result. There are two further dimensions to consider: the offset from the nominal surface, and the width. These can now be compared with the other length scale features.

The offset should be considered carefully. The main problem is that an offset is necessary to ensure that pores cannot intersect the surface. Using the heuristic model creation tool, varying the offset cannot be considered without also considering varying the maximum pore dimension, because the offset defines the allowable position of the centre of the pore, so that larger pores can extend further towards the surface than smaller ones. In view of this, perhaps the issue of relative size of the offset and the maximum pore size can be addressed by the same computational experiment, *viz.*: varying the maximum pore diameter.

> **Resolution 2a:** vary the size of the maximum pore diameter by about an order of magnitude, for the same offset dimension.

Finally, let us consider the width of the defined zone area. This is similar to considering the number of pores that can be placed within the defined zone. Geometries with small pores with close packing would look similar to scaled versions of geometries with larger pores and a wider defined zone. In this case, the major difference would be in the scale of the offset and the surface roughness profile; however, those differences are separated from the left hand side of the defined zone by the presence of multiple pore features. Those features and Saint Venant's principle would suggest a sufficient separation of detail, as to suggest that there would be little length scale interaction between defined zone width and details at or near the surface.

> **Resolution 2b:** disregard this issue in the present study.

3.3 Effect of pore size and position

There are two parts to this issue: the first is to address the effect of large pores versus smaller ones, and the second is consider the role of pore size for pores situated deeper into the body of the material. Taking the second issue first, it should be noted that in this paper porosity is considered as a near surface phenomenon, rather than an effect on the entire material bulk [56]. As a surface phenomenon, it is reasonable to consider the presence of porosity to a maximum depth into the sub-surface, and it is also reasonable to suggest that this is achieved by making the pore diameter shrink to zero towards that limiting depth. For a thorough assessment, it might be ideal to allow the pore size to be randomly assigned, but with a distribution rule, such that the mean pore size is related to the pore depth into the sub-surface.

> **Resolution 3a:** apply a simple linear relationship to fix pore diameter for each pore depending on pore depth. (Random assignment of pore diameter, or other interpolation schemes, could be addressed in future work.)

Having determined that the pore size at any depth in the sub-surface can be fixed in proportion to its depth, there remains only one variable, which is the maximum pore diameter.

> **Resolution 3b:** vary the size of the maximum pore diameter by about an order of magnitude, for the same surface profile.

3.4 Effect of porosity volume fraction

In the typical manufacturing context, porosity volume fraction is a measure of the void content in a bulk of material. It is somewhat difficult to apply the same measure to porosity within the sub-surface, and to ensure that the characterisation method is meaningful: this will be discussed in Section 4.3.3. In this paper, the aim has been to ensure that the porosity is distributed as evenly as possible, using the Spacing Factor to exclude pores from approaching too closely, and by making multiple attempts to place pores.

> **Resolution 4:** vary the value for the Spacing Factor by about an order of magnitude, for fixed maximum pore diameter.

3.5 Effect of porosity distribution

There are two ways in which the porosity distribution could be varied: systematically, or randomly. In regard to systematic variation, the present geometry creation scheme relies on using the same value of Spacing Factor for each pore within any individual model created. This means that in relative terms, the porosity volume fraction reduces with depth into the sub-surface. Varying the Spacing Factor, and/or varying the relationship between pore location and pore size, would lead to a systematic change in the local porosity distribution.
Random porosity distributions could be achieved by using smaller values for the Spacing Factor, thereby allowing closer approach, but reducing the number of trial pore placements, so that the distribution is not *"fully dense"* [57-58]. Such a scheme might also provide a means for characterising the nature of the porosity; however, results reported to date are qualitative rather than quantitative.

> **Resolution 5:** postpone the consideration of the effects of systematic and random variation in porosity volume fraction for a later publication.

3.6 Continuum mechanics limit

We recognise that this is an area which deserves further consideration, particularly if it becomes clear that the mathematics of fractals becomes significant part of the developing understanding. For the moment, we consider *"fractal"* to be limited in length-scale to that which is feasible to model using Finite Element Analysis. We also assume that the notional *"small crack"* which forms the basis of fatigue analysis is related in some way to the observable length-scale features of the surface profile and sub-surface: *i.e.* typical distances between the bigger surface troughs, and size and spacing of pores and flaws within the sub-surface. On that basis, the continuum mechanics limit will be considered as being out of scope for this paper.

4. MODELLING APPROACH

To investigate the influence of both surface finish and sub-surface porosity a series of 2D models were created. These were based on the concept of a simple test specimen, either containing sub-surface porosity, or having a rough surface, or both. Figure 2 indicates a typical geometry for a test specimen, an enlarged image of the gauge section (the region in which a specimen would be expected to fail under test), the modelled region, and a further enlarged image showing the detailed area of model as will correspond to the geometry construction diagrams in later figures.
In all figures, the rough surface/porous sub-surface is shown vertically on the right, and is intended to be indicative of roughness at the edge of the specimen gauge section. The model assumes 2D plane stress and mirror symmetry. Additionally, on the basis of Saint-Venant principle [71], detailed modelling of the geometry and loading is unnecessary at a sufficient

distance from the region of the model of interest. On this basis, the FEA model could be reduced to the form indicated in Figure 2(c).

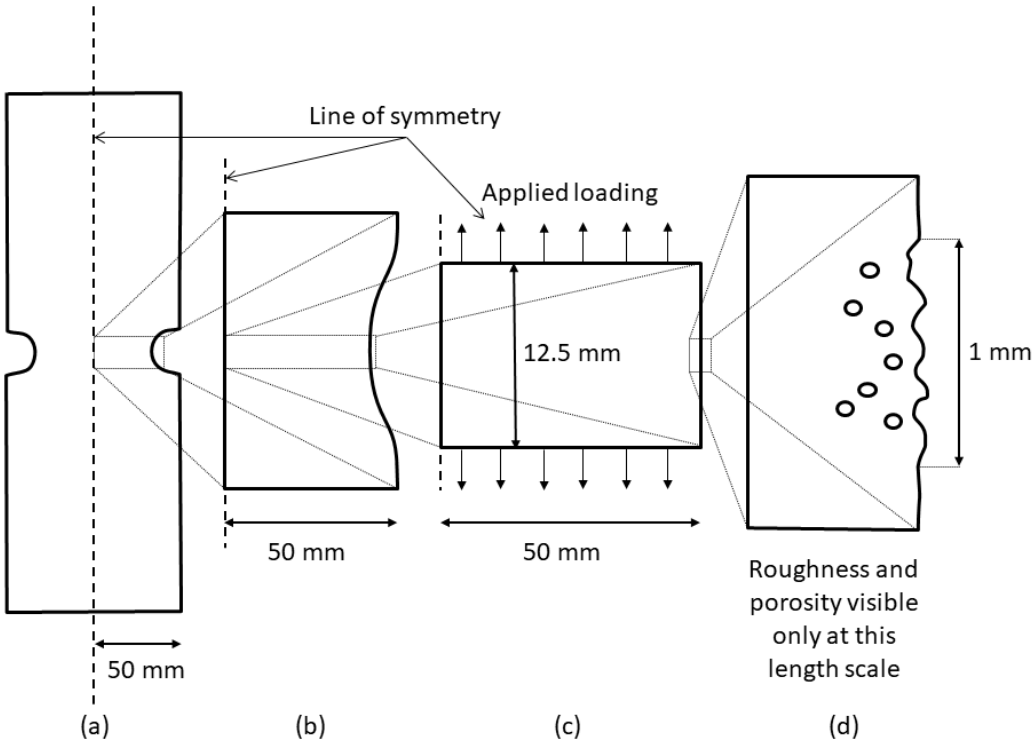

Figure 2. Sketch of model geometry in the context of a test specimen, N.B. aspect ratios are not drawn to scale: (a) Test specimen, (b) Gauge section of test specimen, (c) Model geometry, and (d) Region of interest of the model.

4.1 Material properties, assuming homogeneous

The material properties used for every analysis are shown in Table 1. These properties are not real data, but are fairly representative of steel, and were taken from an analysis example given in the Abaqus Manuals [69]. Notice that the plasticity model is a piece-wise linear strain-hardening model, such that initial yield takes place at a von Mises stress of 300 MPa, and that subsequent higher stresses are supported at the given corresponding plastic strain levels.

Table 1. Material properties used in the computational simulation.

Elasticity definition		Plasticity definition		Legends	
Young's modulus	Poisson's ratio	Stress (MPa)	Plastic Strain	Figure 5	Figure 6
210 GPa	0.3	300 350 375 394 400	0.0 0.025 0.1 0.2 0.35	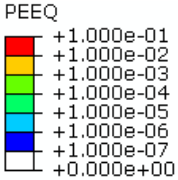	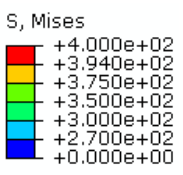

The legends for all of the stress and strain results are all the same, and are included in this table also. Notice that the stress results are of von Mises stress, and the contour intervals are as defined by the strain-hardening model step intervals. The equivalent plastic strain results, denoted PEEQ in the Abaqus finite element results output, are displayed in this paper using a logarithmic scale.

4.2 FEA modelling

The finite element model comprises only a small part of the overall geometry, but included significantly geometry than is shown the results images. The sketch suggested in Figure 2(c) is not drawn to scale, but it does represent the mirror symmetry on the left hand side edge, and the applied loading, as distributed pressure, on the upper and lower surfaces. In addition, minimal boundary conditions were applied to satisfy the rigid body requirement, without any additional constraint.

The element mesh size in the region of interest was very fine. This was to satisfy the need to represent a finely graded surface roughness profile, the varying sizes of pores, and the need to represent the stress-strain state to a good degree of fidelity. Away from the region of interest, a much coarser mesh was sufficient, and to ensure a suitably smoothly graded mesh transition a systematic approach to geometry partitioning was employed. This approach has been described by the authors in more detail in a previous work [63].

Table 2. Model information.

Parameter	Value	Unit
Half-width of the specimen at the nominal gauge section	50×10^{-3}	m
The modelled height (within the gauge section)	12.5×10^{-3}	m
The modelled roughness band and defined zone height	1×10^{-3}	m
The modelled defined zone width	0.3×10^{-3}	m
The modelled defined zone offset from the nominal surface	0.1×10^{-3}	m
Typical roughness feature dimensions	$\leq 0.1 \times 10^{-3}$	m
FEA mesh seed size in the roughness region	3.125×10^{-6}	m
FEA global mesh seed size	0.25×10^{-3}	m
Applied pressure load, equal to nominal uniaxial stress state	$\pm 270 \times 10^{6}$	Pa

The load applied was ±270 MPa, which for a perfect specimen without surface or porosity features would represent von Mises stress of 90% of yield. In other words, the strain would be completely elastic and fully reversible. The effect of the surface roughness or porosity features is to create localised stress raisers, which lift the local stress field into the plastic regime. Subsequent reverse loading and reloading cycles develop the local plasticity zones. As the purpose of this study is to consider how this repeated loading might contribute to our understanding of fatigue life, in the analyses presented here multiple loading steps were defined, to give five fully reversed half cycles.

The particular model information is presented in Table 2. This provides both particular dimensional information as well as indicative mesh size information.

4.3 Geometry creation

A heuristic geometry creation tool is described, that can generate multiple example geometries, "computational specimens" that can subsequently be modelled and analysed using finite element analysis.

The surface roughness was defined randomly at 12.5 μm intervals, in a range of ±50 μm from the nominal surface, using the same method as described in [63]. In the current paper, the

profile is defined by a discrete set of points, through which a spline interpolation is fitted. In [63] it was established that the choice of interpolation scheme made little significant different to the stress and plastic strain distribution in the sub-surface region. This same surface profile was used for each model. The test of randomness and scale variation was addressed by introducing variation in the porosity configurations.

There are considerable geometry handling issues with the definition of porosity. The requirement that this paper sets out to address is the generation of geometry that has some reasonable similarity with the size of porosity and lack of fusion (LOF) regions observed in real additive manufactured products. It has to be admitted that a region of LOF is not the same as a perfectly circular void, but it is necessary to keep the model simple in the first instance. If one considers the effect on the load path, then the approximation may not be unreasonable. The generation of the circular pores is illustrated in Figure 3. The centres of the pores are placed randomly within a defined zone of the model, which is the 0.3 × 1 mm rectangle shown in dashed lines.

To satisfy **Resolution 1**, the tool must be capable of generating similar geometries with similar porosity volume fractions, and to achieve this, the distribution of the pores was controlled by an exclusion method [56]. The coordinates of the pore centres were generated randomly, then as each consecutive pore was placed its distance from previously generated pores was checked. If that distance was too small then the pore would be rejected from the model, and the next coordinate pair would be assessed. In Figure 3, this is illustrated by the exclusion zone circles, and it can be seen that no such circles can intersect. One limitation of this method is that the computer program that embodies it must be finite: only a finite number of pore generation attempts can be made. For small numbers of large pores, it is readily possible to be assured that for any instance of a random distribution of pores, it would be impossible to add an additional valid one: *i.e.* this is *"fully dense random packing"*. For larger numbers of smaller pores this becomes increasingly difficult to be sure to achieve, even for very large numbers of pore placement attempts. The significance of achieving this *"fully dense"* packing is that the resulting porosity distribution is *"homogeneous"* [57-58]. It should also be noted that, because of the random nature of the pore placement process, it is possible for somewhat different levels of porosity and numbers of pores for different "computational specimens" produced using the same parameters.

The defined zone is set back by 0.1 mm from the nominal surface to avoid the possibility of a pore breaking through to the surface: this is a requirement of **Resolution 2a**. In reality, it is quite possible that such a pore break-through would then lead to the creation of a new surface profile feature: so while in the modelling world we can differentiate between pores and surface profile, in reality these would be inter-related.

In this model, to meet the requirement of **Resolution 3a**, the diameter of the pores has been set to be linearly proportional to the distance from the left hand edge of the defined zone. The remaining requirements of **Resolutions 2a** and **3b** are achieved by varying the Maximum pore diameter variable, while the requirement of **Resolution 4** is met by varying the Spacing factor.

4.4 Computational specimen test matrix

A test matrix was created, based on the geometry definition requirements, constraints, and variables identified by the scheme of Resolutions. For the purposes of this paper, the only variable parameters are the Maximum pore diameter and the Spacing factor. The heuristic tool can be used to create a number of "computational specimens" for each set of parameters: in this case three models were created for each parameter set for which a full FEA cyclic loading analysis was carried out. A further 50,000 geometries were computed for statistical assessment of porosity volume fraction and the number of pores count.

In summary, these studies:

- Use the same surface profile for each model
- Vary the maximum Pore Diameter, for fixed Spacing Factor
- Vary the Spacing Factor, for fixed maximum Pore Diameter
- Create three models for each trial, for full FEA analysis
- Create 50,000 geometries for each trial, for statistical assessment

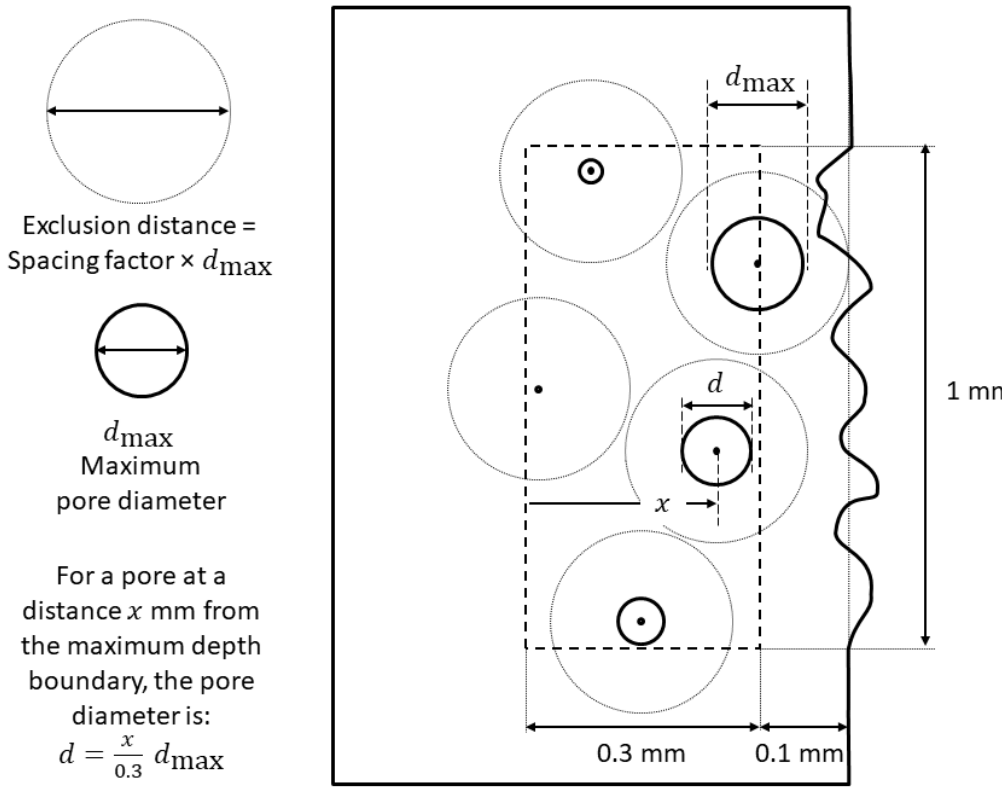

Figure 3. Pore size and placement

Based on these a computational specimen test matrix was planned, with model parameters as set out in the first three columns of Table 3. This comprised 3 × 7 = 21 computational models.

Table 3. Computational Specimen Test Matrix and PEEQ Penetration Results

Maximum Pore Diameter (µm)	Spacing Factor	Exclusion Distance (µm)	**Penetration distance results (µm)** [Left to right in correspondence with images in Figures 7 and 8]		
25	3	3 × 25 = 75	502 (±14)	513 (±6)	512 (±7)
50	3	3 × 50 = 150	532 (±19)	562 (±18)	543 (±15)
75	3	3 × 75 = 225	540 (±18)	543 (±11)	603 (±19)
100	3	3 × 100 = 300	633 (±15)	629 (±8)	730 (±4)
50	2	2 × 50 = 100	636 (±8)	656 (±16)	643 (±16)
50	4	4 × 50 = 200	512 (±15)	537 (±14)	442 (±14)
50	5	5 × 50 = 250	436 (±3)	456 (±6)	447 (±14)

4.5 Statistical repeatability and calculation of *"porosity volume fraction"*

The geometry for the models was created using a Python script. Python is the underlying language for the Abaqus CAE tool (the pre-processor for the Abaqus package), so this programme enabled much of the geometry creation and meshing activity for the finite element models to be undertaken automatically.

While it is reasonably possible to create large numbers of example models, it is less reasonable to analyse each of them and present all of those results, but it is reasonable to question the statistical variation between results. To do this efficiently, the Python script was modified, to remove the Abaqus specific instructions, and to carry out some additional calculations for number of pores, total area of pores, and the *"porosity volume fraction"* defined as being the total area of the pores divided by the defined zone area.

Because the calculation for porosity volume fraction was based on the area of the defined zone for pore centres, it is clear that this definition is inadequate, because it fails to recognise that pores near the edges of the zone can overlap. This problem is illustrated in Figure 4. The error is particularly significant for larger maximum pore sizes.

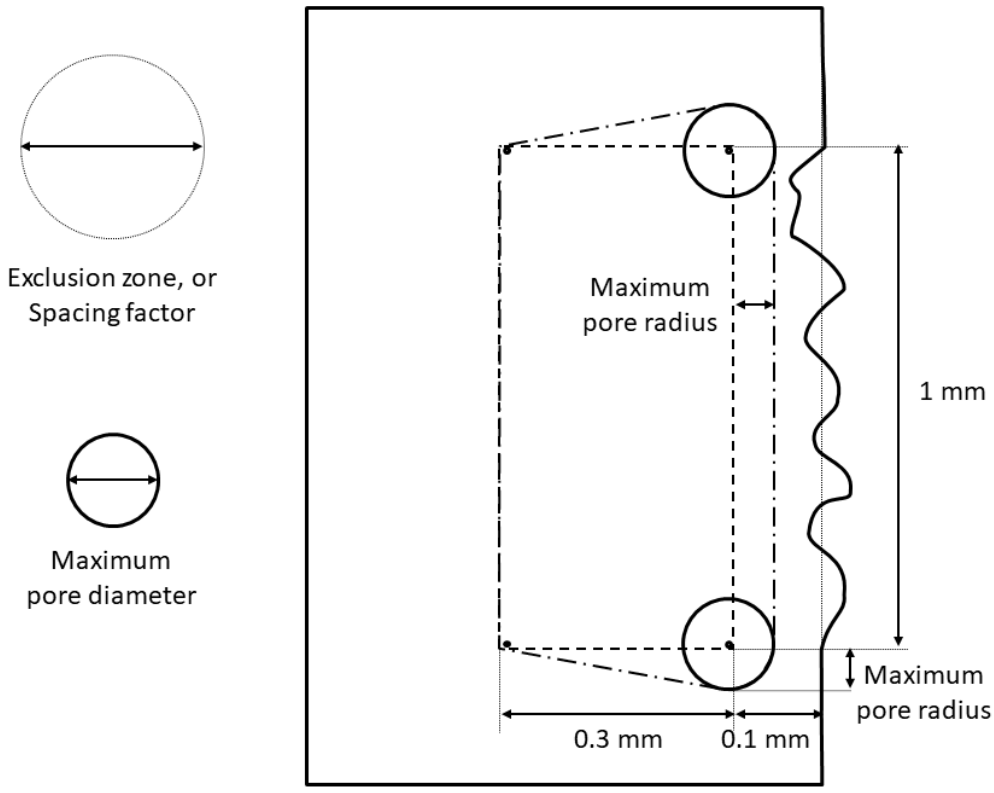

Figure 4. Illustration of the difficulty in establishing baseline area for the porosity calculation

A simple correction of the error, using the area defined by the dash-dot outline (Figure 4) can be calculated; however, this correction is almost linearly proportional to the maximum pore diameter (with a small squared component for the two quarter circle regions), so it only represents a re-scaling of results. Furthermore, this correction is insufficient, because it fails to recognise the effect of there being no neighbouring pores with centres outsize the defined zone, to provide an exclusion zone effect. The result of this is that pores are disproportionally more likely to appear near to the edges of the defined zone. The effect of such disproportional appearance of pores near the upper and lower boundary of the defined

zone will have some influence on the appropriate value for the porosity calculation. A more significant effect arises from the disproportional appearance of pores near to the right hand side, *i.e.* immediately in the sub-surface area. It is an effect that will be difficult to quantify, and is an unintended consequence of the pore placement heuristic. Having pointed out this failing, it is also necessary to remark that all these effects become less significant for the placement of larger numbers of smaller pores.

5. RESULTS OF THE COMPUTATIONAL EXPERIMENTS: A. SIGNIFICANCE OF MODELLING BOTH SURFACE PROFILE AND SUB-SURFACE POROSITY

There are two parts to this paper. The first part concerns the significance of modelling both surface profile and sub-surface porosity. The second part is concerned with the effects of relative pore sizes and levels of porosity for a reasonably homogeneous porosity distribution: this will be addressed in Section 6 and thereafter.

5.1 Description of the models

In this first part, three models were created: (a) a model with a rough surface profile, (b) a model with sub-surface porosity, and (c) a model which combined the rough surface profile and the sub-surface porosity.

For each model, equivalent boundary conditions and five half cycles of fully reversed loading steps of ±270 MPa pressure were applied. The mesh size in the neighbourhood of the surface profile and porosity features was controlled to be similar in each case. In a similar previous study [63] it was found that the basic stress and equivalent plastic strain pattern was established after the first load, and the development of those patterns became clear after only a few half cycles.

A further model with neither roughness nor porosity is unnecessary, as the result is analytically obvious. In this case, the state of stress is constant through the whole model, and equal to the applied pressure, ±270 MPa. Since the yield stress is never exceeded, there can be no plastic strain even after multiple reverse loadings. An equivalent nominal stress state is seen in each of the other models at Saint Venant distances from the stress raising features.

5.2 Computational results

The results are shown in Figure 5 for equivalent plastic strain (PEEQ), and in Figure 6 for von Mises stress. The model configuration is similar to that illustrated in Figure 2(d), with the area shown just including the roughness and sub-surface porosity region, *i.e.* an area of 0.55 by 1 mm. The results from left to right indicate the state of PEEQ or stress following each of the five half cycles of loading.

As is self-evident, the top rows of both figures show the effect of roughness only, the middle rows show the effect of porosity only, and the bottom rows show results where both the roughness and the porosity are modelled. The legends for these figures are given in Table 1. Figure 5 is plotted on a logarithmic scale, down to the grey region showing equivalent plastic strain of less than 1×10^{-7}. In the case of Figure 6, the von Mises stress colour bands indicate the steps in the material definition so that the boundary between dark and pale blue is equivalent to the nominal state of stress, 270 MPa. As the elements of the model are tiny, the mesh lines have been suppressed, but an impression of the mesh size is given by allocating one colour per element.

It is clear from the results that the combined effect of both surface roughness and sub-surface porosity leads to a greater sub-surface penetration of local plastic strain than is the case where

either surface roughness of sub-surface porosity is considered alone, see Table 4. Additionally, the level and extent of the plastic strain is also significantly greater when both roughness and porosity are modelled. In all three cases, the level of plastic strain increases with the number of load cycles, but the extent is almost constant.

In Figure 6, the regions of the material for which the yield stress has been exceeded are shown in green. Higher stress values are present in localised regions, but the elements with those results are too tiny for the other colour contour bands to be visible.

It is to be noted that the extent of yield stress region is highest following the first half cycle, and reduces on subsequent cycles. Thus it seems that the effect of load cycling is to redistribute the stress field through the plastic deformation.

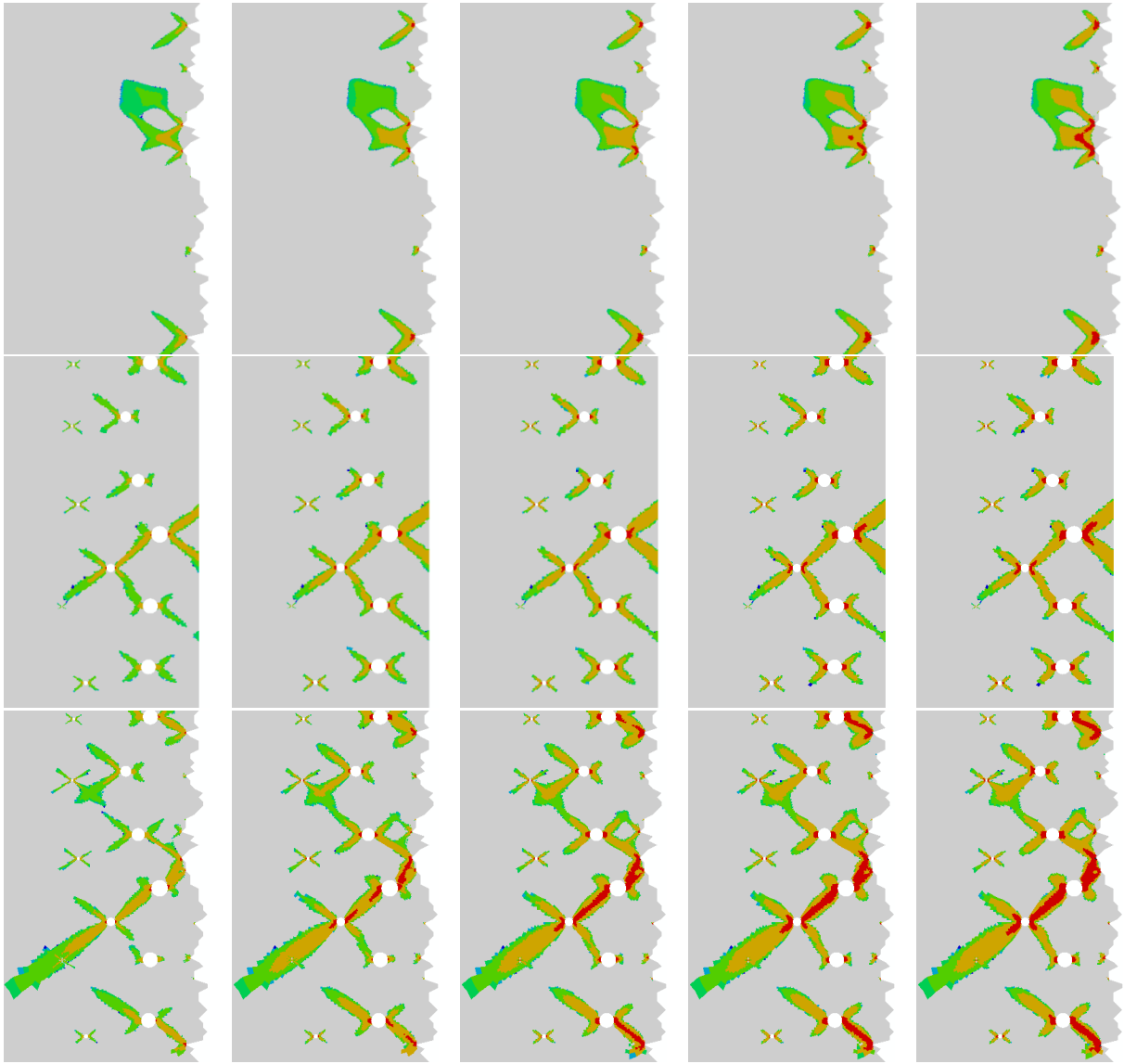

Figure 5. 2D Equivalent Plastic Strain – 5 half cycles (fully reversed).

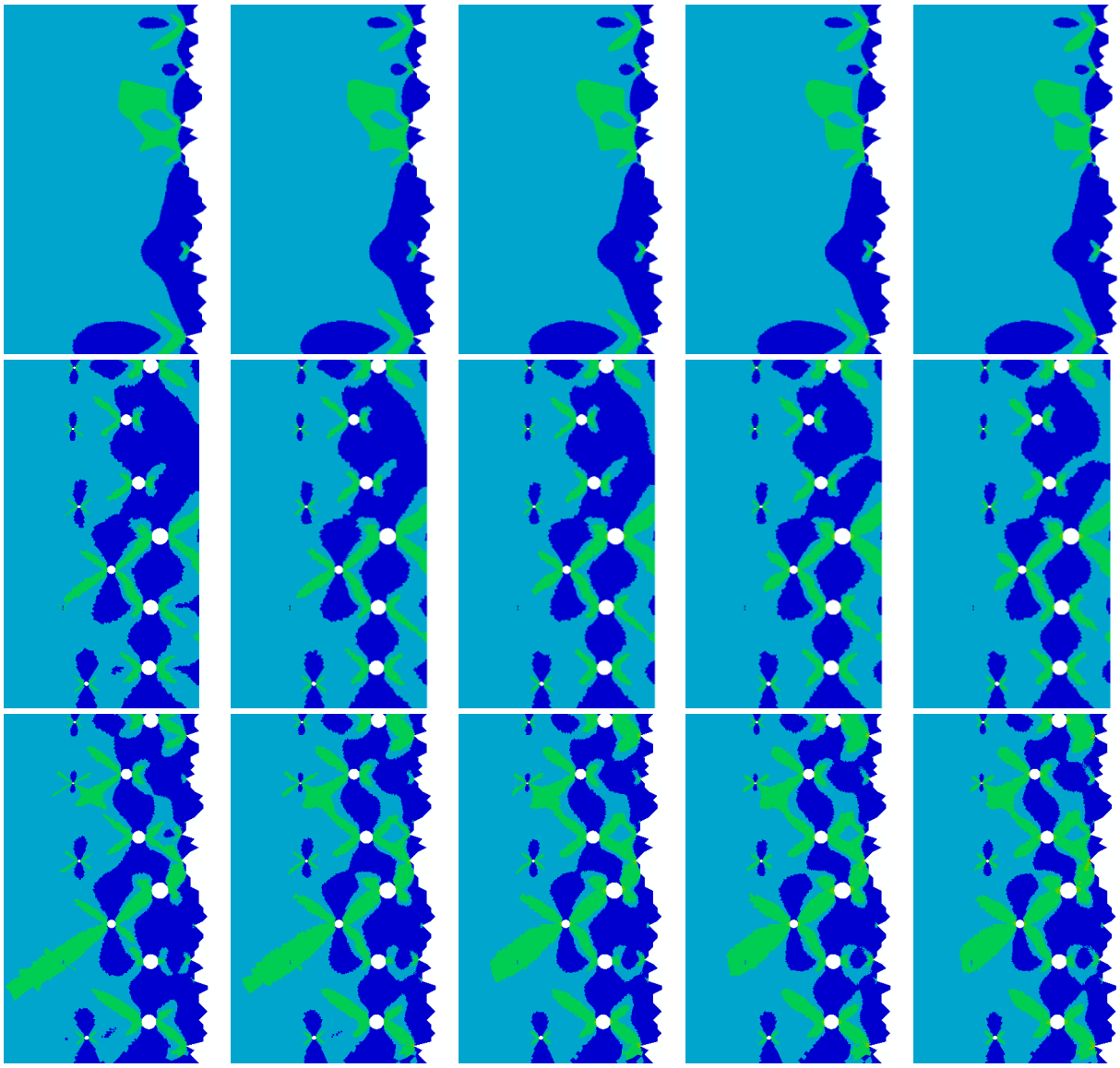

Figure 6. 2D von Mises Stress – 5 half cycles (fully reversed)

Table 4. Plastic strain penetration for different model versions

Model description	PEEQ penetration depth	PEEQ pattern
Surface roughness only	0.25 mm	Isolated, rounded
Sub-surface porosity only	0.4 mm	Partially networked
Combined surface roughness and sub-surface porosity	0.55 mm	Almost fully networked with higher PEEQ values

6. THE COMPUTATIONAL EXPERIMENTS: B. EFFECTS OF VARIATION, LENGTH SCALE, RELATIVE PORE SIZE AND DISTRIBUTION

Given that the importance of modelling both the surface profile and the sub-surface porosity is established, the next step is to examine the effect of variations and length scales in the models.

Examining the results presented above, we see that the von Mises stress (S, Mises) and equivalent plastic strain (PEEQ) results show similar features. The PEEQ information is perhaps more useful as it indicates accumulated strain. This means that the magnitude of the results increase with increasing numbers of half cycles. For the von Mises stress results, the effect of plastic strain is to unload the stress raising features, so the magnitude of difference these results to the nominal stress gets smaller with increasing numbers of half cycles, and local regions where plasticity has occurred can show as having lower stress after multiple cycles than the yield stress. On that basis, results from hereon are presented as PEEQ, at the 5^{th} half cycle.

6.1 Results from models with varying maximum pore diameter

The results presented in Figure 7 show the results from the 12 computational models for which the spacing factor was set to be 3. For each row, the first three images show equivalent plastic strain (PEEQ) results after the 5^{th} half cycle of loading. The pattern of pore distribution is self-evident, but it should be noted that the models are arranged in order from left to right in order of increasing pore void area. Because the mesh for these models is so fine in the regions local to the pores and surface features, the mesh lines have been suppressed, but results have been displayed using the *"Quilt"* option, so that elements are shown as a single colour, rather than as an interpolation. This makes the larger elements visible at the edges of the PEEQ zones.

6.2 Results from models with varying spacing between pores (fully dense)

The results presented in Figure 8 show the results from the 12 computational models for which the maximum pore diameter was set to be 50 μm. Notice that the models shown in row (b) are repeated from Figure 7, but shown here for their position in the context of varying the spacing factor.

6.3 Assessment of the statistical distribution *"porosity volume fraction"*

The images shown in the right hand columns of Figures 7 and 8 are statistical distribution measures of the *"porosity volume fraction"*, as defined in Section 4.5. In addition to the mean and standard deviation data for *"porosity volume fraction"* the mean and standard deviation for the number of pores is also given. These were obtained based on data calculated from 50,000 model geometry creations for each combination of maximum pore diameter and spacing factor. The white dashed lines represent the approximate position in the distribution of the three models shown to the left, for which the FEA analysis was carried out. The porosity distributions can be seen to be sensibly similar to Gaussian for most cases except for the larger maximum pore diameter, Figure 7(d).

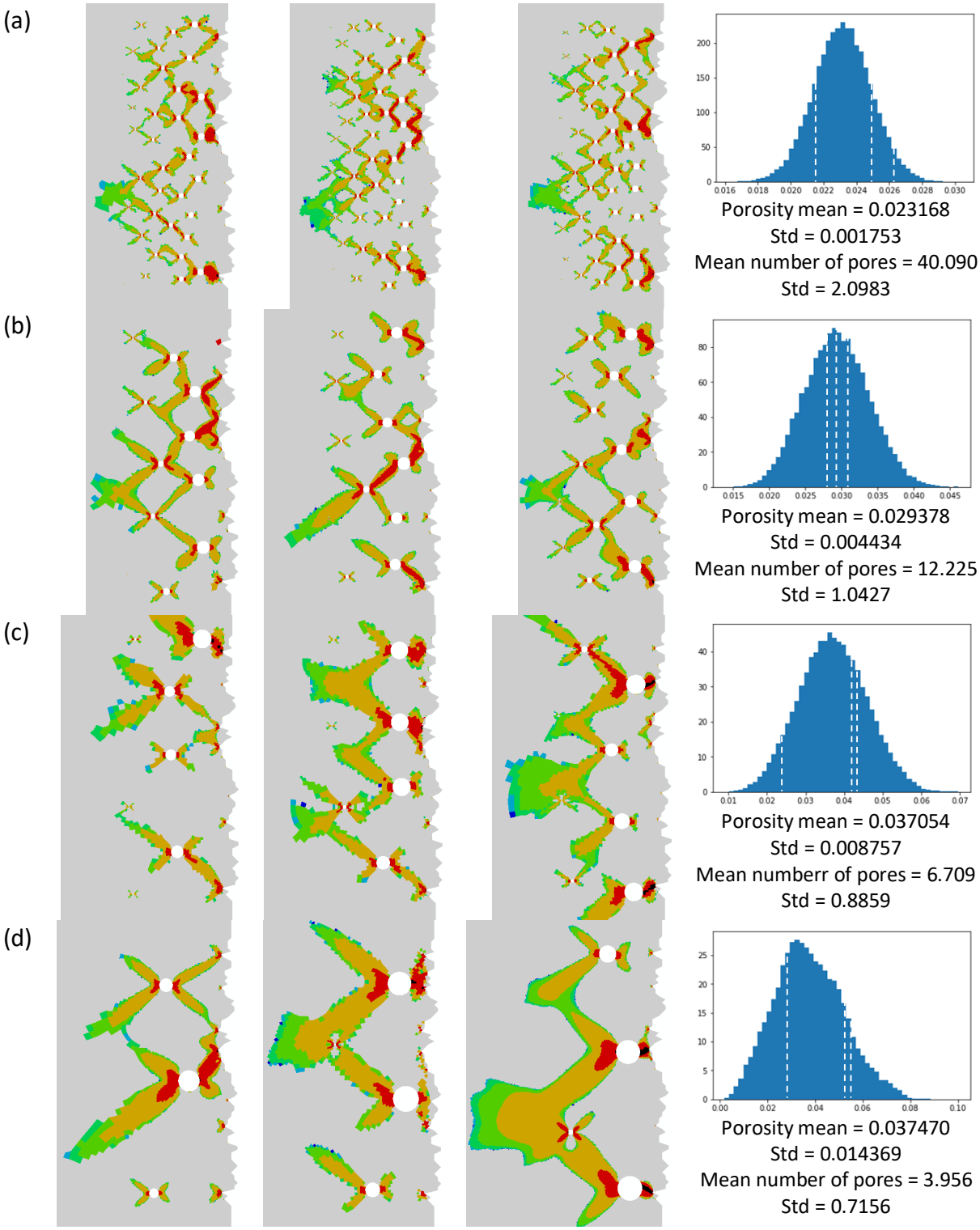

Figure 7. PEEQ distribution for varying maximum pore diameters: (a) 25 µm, (b) 50 µm, (c) 75 µm, (d) 100 µm. In each case, the spacing factor was 3.

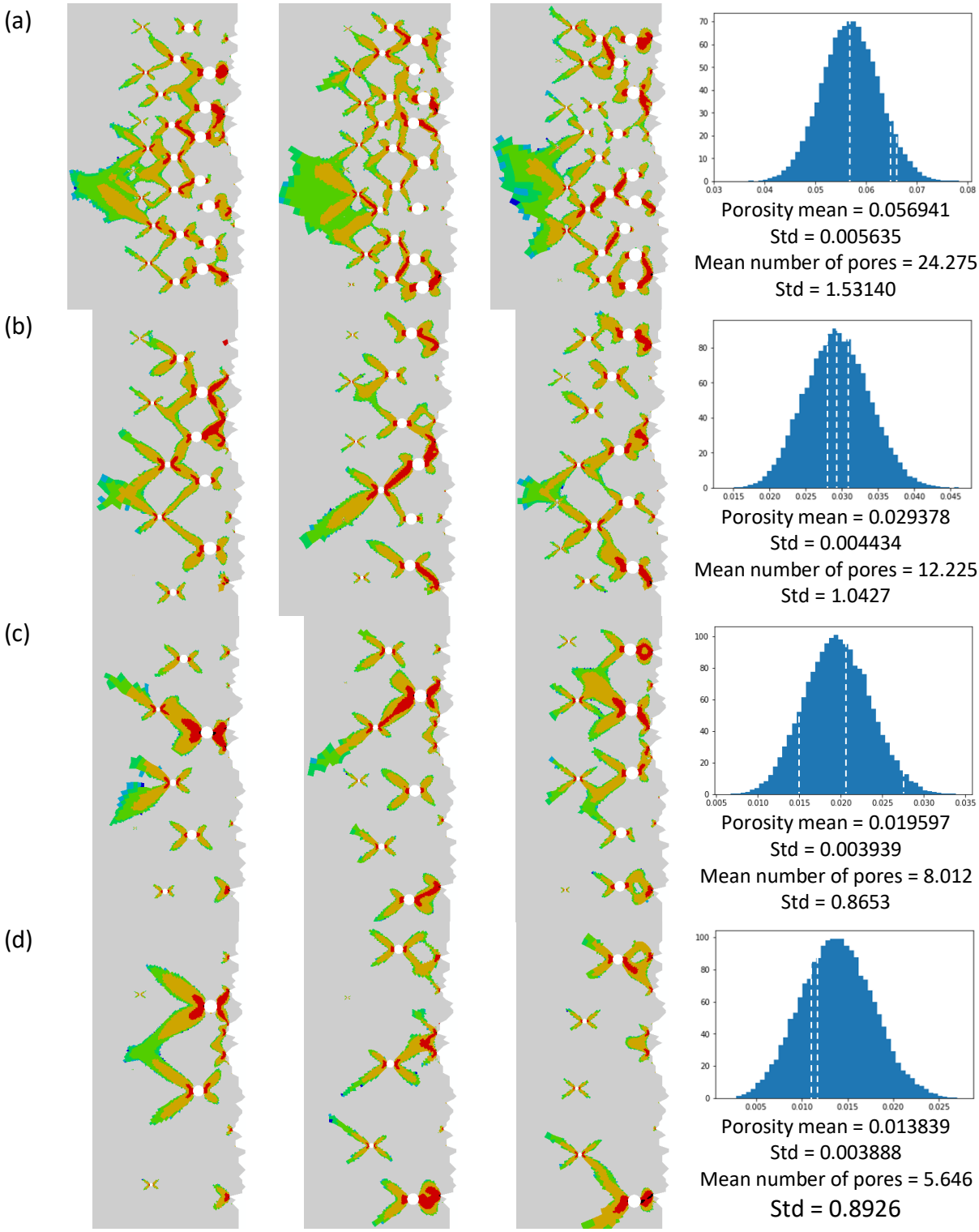

Figure 8. PEEQ distribution for varying spacing factor (a) 2, (b) 3, (c) 4, (d) 5. In each case the maximum pore diameter was 50 µm.

6.4 Graphical analysis of results

In presenting the results it would be tempting to try to correlate penetration depth with porosity, but as discussed previously, porosity is difficult to define in a meaningful way. The meaningful variables are those used to drive the heuristic model geometry definition tool, namely the maximum pore diameter, the spacing factor and the exclusion length, which is the product of the first two.

The analysis results quantity, PEEQ penetration depth, is tabulated in the right hand columns of Table 3. The values shown from left to right correspond with the FEA analysis result images shown in Figures 7 and 8. The penetration depth was measured from the FEA results by identifying the left-most element having a PEEQ value greater than 1×10^{-7}, in other words, the left-most coloured element. The left-most and right-most nodes of that element were examined, and the PEEQ penetration depth set equal to the average, and the ± error being half the difference. This is illustrated in Figure 9.

The results shown in Figure 10 compare the effect of maximum pore diameter on the PEEQ penetration depth, for constant spacing factor, equal to 3. The data plotted corresponds to the first four rows of Table 3, with three data points per maximum pore diameter result. The error bar for each individual result was determined using the above method, and for that reason, each result has a somewhat different error bar size. It should be noted that this error is attributable to the particular geometry mesh only: since the geometries are randomly created, there should be no expectation that the results for different geometries created using the same parameters should be equal to within a tolerance defined by these error bars. The dashed line shows the linear trend of the combined results.

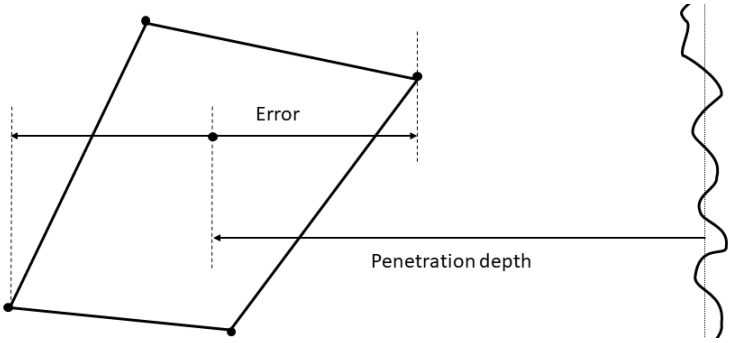

Figure 9. Schematic of the PEEQ penetration depth result interpretation method.

Figure 11 shows the effect of spacing factor on PEEQ penetration depth, for maximum pore diameter equal to 50 μm. This data corresponds to the last three rows of Table 3, and is shown using white markers with a black outline. The data set of the fourth row of Table 3, being common to both Figure 10 and 11, is shown with solid black markers. The dashed trend line suggests an inverse relationship.

The complete data set is presented in Figure 12, for maximum pore diameter divided by the spacing factor. Each parameter set is shown using the same marker shape and colour as used in Figures 10 and 11. Again, the dashed line shows the linear trend.

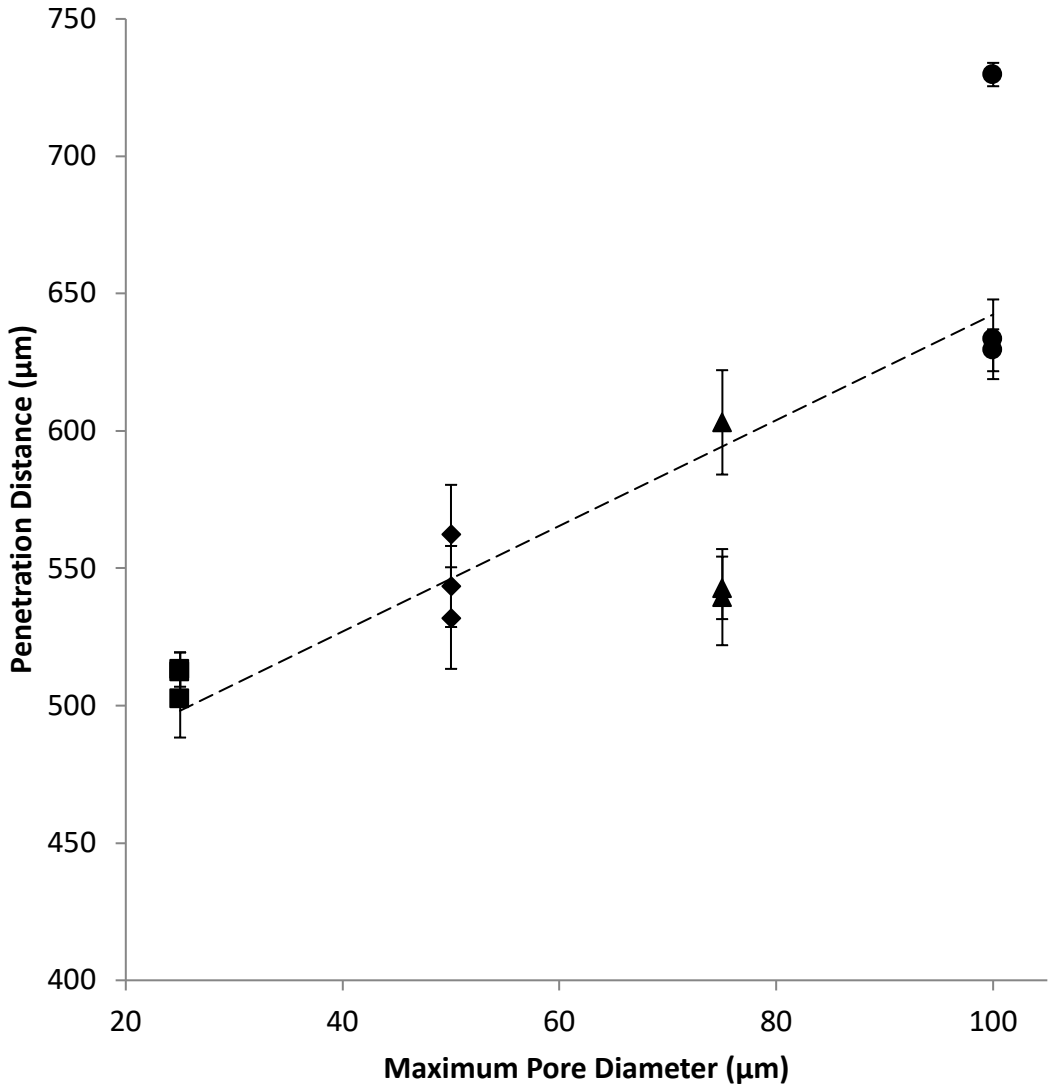

Figure 10. Effect of Maximum Pore Diameter on PEEQ penetration depth. Spacing Factor = 3.

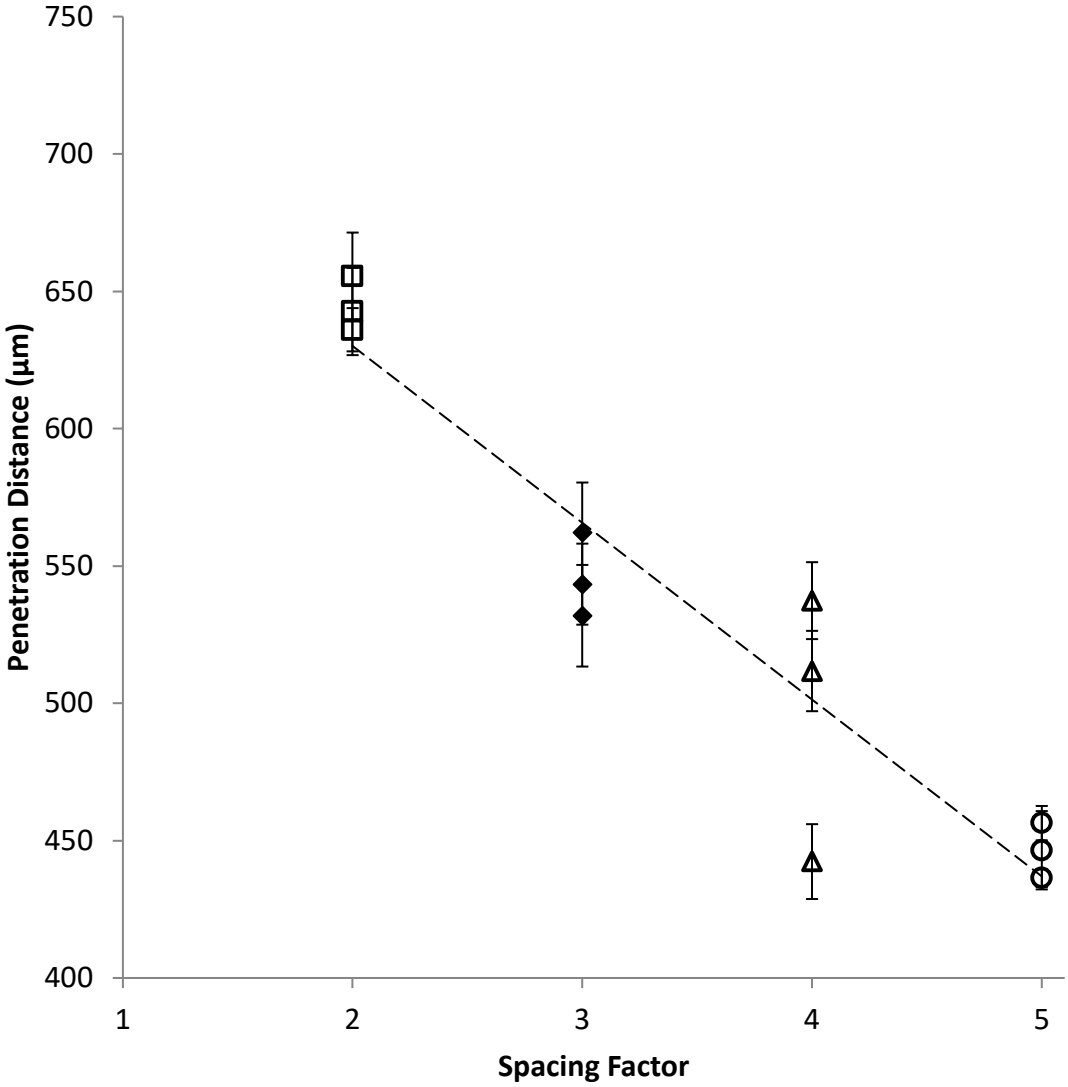

Figure 11. Effect of Pore Spacing Factor on PEEQ penetration depth. Maximum Pore Diameter = 50 µm.

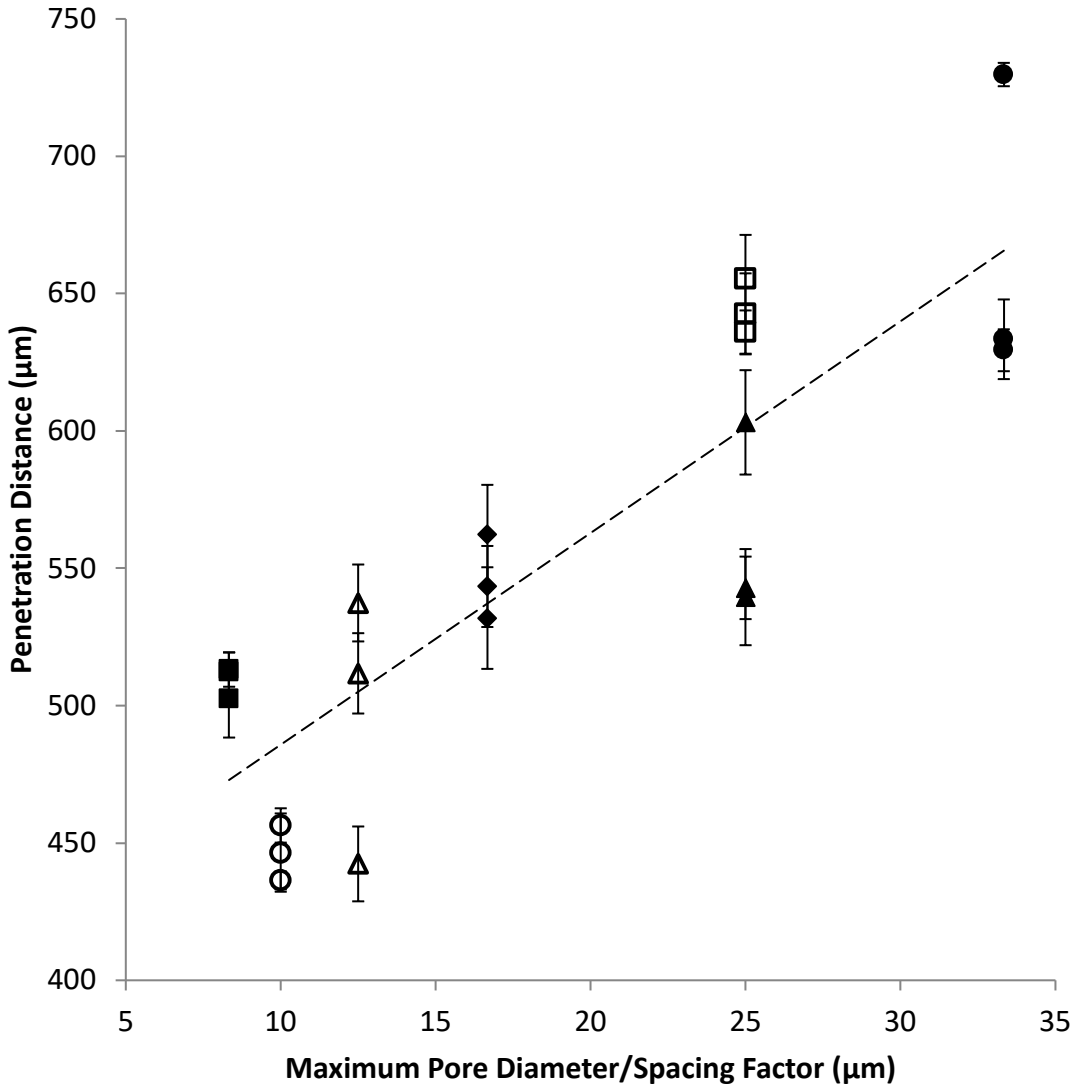

Figure 12. Maximum Pore Diameter and Spacing Factor effects amalgamated onto one chart, by plotting Maximum Pore Diameter / Spacing Factor against PEEQ penetration depth.

7. DISCUSSION

7.1 Form of the results

The results presented here are of three different types.

7.1.1 Significance of modelling both surface profile and sub-surface porosity

First, there are results presented in Sub-section 4.2. In this case, three models were created from two special geometry sets: a geometry defining the surface profile, and a geometry defining one particular sub-surface porosity configuration. The results presented include both von Mises and PEEQ distributions, and show how those distributions are modified over multiple reverse loading cycles. The results tell us that if both surface profile and sub-surface porosity are taken into account in the model, then the von Mises stress and PEEQ distributions are substantively different in form, and have greater depth penetration, than for the equivalent results for models where only the surface profile or only the sub-surface porosity is modelled.

7.1.2 Statistical results and particular examples

The second type of result presented comes from statistical analysis of multiple geometry creations. The purpose of this computational experiment was to determine whether the heuristic tool for porosity geometry generation was creating models that had satisfactory statistical properties. Given that this is the first attempt to make a systematic approach to modelling random geometry, FEA computational costs were kept small, meaning that domain size had to be minimal, and FEA mesh refinement limited. On that basis, true *"porosity"* would be ill-defined, so the statistical analysis was performed on the stand-in measure of *"nominal porosity"*, equal to the total pore area of the model divided by the pore placement area, as illustrated in Figure 4. Those results are shown in the right hand columns of Figures 7 and 8. It is clear that for most parameters, the distributions are well-defined, and the actual geometries used in the FEA modelling are fairly well representative of the positions within the distributions. The most telling exceptions to this are as follows:

(i) The clearly skewed distribution in Figure 7(d), for maximum pore diameter equal to 100 μm, and spacing factor equal to 3. The issue here is that the maximum pore diameter is so large that very few pores can be placed. In the subsequent analysis of results, in Figure 10, it is one of these modelled geometries that gives the greatest outlier to the trend line. This particular geometry is the one with the largest *"nominal porosity"*, but it is only slightly greater than that for the middle geometry. Furthermore, while the difference in *"nominal porosity"* between the left-hand and middle geometry is much greater, the PEEQ penetration for these two models is rather similar. In any case where there is random variation, then there is a possibility for extremes to occur – in this case, because there are only a few pores (three or four), the effect of the extremes is exaggerated.

(ii) The third geometry of Figure 8(c), maximum pore diameter equal to 50 μm, and spacing factor equal to 4. This falls well to the right of the standard deviation, and of all the geometries modelled is the most like an outlier. The PEEQ penetration result for this example, is also the biggest outlier to the trend plotted in Figure 11. In this case, although the *"nominal porosity"* for this particular geometry is greater than those for the other two models with the same parameters, the PEEQ penetration is actually considerably lower. This indicates an effect of regularity: the only way that a higher than usual porosity can be achieved is through an arrangement of pores that

comes close to a regular close packing. For that kind of regularity, there is an emergent *"self-shielding"* property whereby the pores themselves act as stress relieving features to their neighbours [56].

7.1.3 Pore placement and scaling effects

The third type of result presented is that of the multiple FEA models, showing PEEQ after five half cycles of loading. The selection of the parameters modelled, FEA meshing techniques, and the form of the results was informed in part by the earlier modelling work.

The results presented in Figures 7 and 8 provide a visual indication of the statistical placement for the 21 particular examples forming part of this study. It is assumed that for each of these geometries, the pore placement is *"fully dense"*, meaning that it would be impossible to find any additional site in which another pore could be sited while still obeying the pore spacing requirements. This was built into the heuristic tool, by allowing for a pragmatic number of extra tries, and can also be verified by eye by inspection of the actual models. There is a possibility that there would be non *"fully dense"* examples in the statistical trials.

The FEA PEEQ result figures not only indicate the placement, but also the way in which such placement leads to the particular form of the PEEQ distribution. There are clear differences in scale from one row of results to the next, but the interconnected diagonal lattice form is common to most of the figures. In some cases, the interconnectedness is more complete than in others, but where there is good connection from right to left, this seems to lead to the greater PEEQ penetration results.

For the smaller maximum pore size and smaller spacing factor results, the interconnection does not have to span the domain top to bottom in order to achieve interconnectedness from right to left. In these cases, there is more of a tendency to form a "<" shaped wedge, defined on the right hand side by some of the deeper furrows in the surface profile, and spanning chains of multiple pores, to intersect at the PEEQ penetration depth. It seems that the deepest PEEQ penetration occurs in those models for which there are near surface pores close to deeper furrows, but it should also be remembered that such a placement of those pores does influence the possible sites of neighbouring pores. In Figures 7(a) and 8(a), the particular pore configuration seems to make very little difference to the position and size of the "<" wedges or the region where the greatest PEEQ penetration occurs: these seem to be directly influenced by the positions of the deeper furrows in the surface roughness profile. The two relatively close deeper furrows in the upper third of the domain seem to promote less PEEQ penetration than the pairing that spans the lower two thirds of the domain: in both cases, the penetration depth seems to be approximately the same as the distance between the furrow pairs forming an approximate equilateral triangle. This seems to be a counter-intuitive, emergent result.

For the larger maximum pore diameter and the larger spacing factor models, there are significantly fewer pores in the models, so the formation of chains of pores cannot happen. For the larger maximum pore diameter models, Figure 7(d), the combined coincidence of there being two pores near to two of the deeper furrows seems to be the most significant factor in the PEEQ penetration depth, and possibly that is helped by the placement of a third pore near to the intersection of the PEEQ diagonals behind those two pores.

For the case of the larger spacing factor models, Figure 8(d), there are insufficient pores for interconnected chains to appear. The *"nominal porosity"* and the PEEQ

penetration results for these three models are too similar for discussion of any further feature differences. On inspection of Figure 8(c), a somewhat more interesting picture emerges. Here the *"nominal porosity"* spans the distribution range well. The two left hand models show a diagonal PEEQ chain of two pores, both of which being in reasonable proximity to deeper furrows in the surface, and resulting in similar PEEQ penetration depths. In those two examples, all of the other pores are reasonably well separated from each other. The right hand example, already noted as being an outlier, shows multiple chains of pores, but none of these groupings leads to the perfect diagonal alignment that seems to be necessary for the larger PEEQ penetration achieved by the other two examples. In Sub-section 6.1.2, this effect was attributed to the higher *"nominal porosity"* in this example, and supposing that this was connected with a close packing effect. Looking more closely at the detail, the packing is concentrated in the upper half of the domain, with six pores arranged similarly to the spots on a die. This packing arrangement is dissimilar to the closest packing, which would be hexagonal packing; however, this square packing configuration seems to provide greater stress shielding.

7.2 Meaningful measures: PEEQ penetration and *"porosity"*

The difficulties in defining a measure for porosity have been discussed, and the proxy used in the data analysis, the *"nominal porosity"*, has been defined. The spread of results seems to increase with increasing maximum pore diameter, but it should also be remembered that for the larger pore diameters, there are fewer pores in each model, and therefore a greater variation would be expected. Because the area over which the pores are allowed to fall is poorly defined, any comparison between results from models with different maximum pore diameters and spacing factors must be considered qualitative rather than exactly quantitative. In view of the limited number of result data points, the trend lines given in Figures 10, 11 and 12 are linear trend lines, but there is no intention to imply that there is a strictly linear relationship. Although the data is insufficient to define the relationships exactly, there is a clear trend of increasing PEEQ penetration distance with increasing maximum pore diameter, and of increasing PEEQ penetration distance with decreasing spacing factor.

7.3 Example cases and *"worst cases"* – assume worst case always exists!

The models presented are of limited domain size, and so the value of PEEQ penetration distance represents the value seen in the particular configuration. Had a larger domain been modelled, then there would also be a larger number of pores, and a greater opportunity for the random configuration to give rise to a somewhat larger PEEQ penetration value. The larger the modelled domain, the more likely that it will contain a configuration that leads to high PEEQ penetration depths, and the less likely that it will be entirely comprised of fortuitously aligned pores such as in the right hand model of Figure 8(c).

7.4 Mesh size effects

Since the pores are arranged randomly, it is impossible to define an entirely regular mesh. In so far as regularity is possible, the focus has been on the most critical regions: at the surface, and around the surfaces of the pores. Mesh seeding at the boundaries ensures mesh regularity for the first layer of elements adjacent to the surface. To control mesh properties deeper within the bulk of material, it is necessary to use partitioning. The mesh style around the pores was standardised, using partitioning methods described in [56]: this text also discusses the issues of mesh uniformity and adequacy of mesh choice on pore boundaries. The mesh quality between the pores and between the pores and the surface was less easy to control

automatically, but each mesh was inspected, and judicious use of partitioning made to ensure that elements were of reasonable sizes and shapes.
The elements in the regions close to the boundary and between the pores are so small that it has been necessary to suppress the display of the mesh lines. As the results in the Figures 5, 6, 7 and 8 have been presented in *"quilt"* style, the stress or PEEQ values are shown as constant within each element. Thus, the mesh size variation of the larger elements can be seen by the jagged outline at the colour boundaries. There is some variation in the sizes of these larger elements, both within any particular model, and between models.
The error bars for penetration depth in Figures 10, 11, and 12 indicate such element size variation, and it is clear from these figures that the variation which could be ascribed to mesh choice is generally smaller than the variation between models with the same parameters, and smaller than the trend change. In view of this, it can be assumed that the mesh size control for the models presented here is adequate.

7.5 Weaknesses in the modelling that could be addressed in future

There are many aspects of the geometry creation used in this work that should be questioned. First and foremost, there are many difficulties in generating artificial random geometry while at the same time having some control over the resulting form. The methods described have attempted to provide both variation, and a controllable and quantifiable uniformity. Any improvements or changes to the geometry creation methodology would still need to demonstrate similar control.
The ideal geometry creation method might be to generate the material geometry by modelling all the essential physics of the manufacturing process. This would include fluid flow, solidification, modelling flaws and inclusions and out-gassing, and subsequent finish machining. This would be highly challenging work, and would not be a feasible approach, at least in the near future. Another approach would be to take samples of real material, and image it using X-ray Computed Tomography, and construct the CAD geometry from that data. This would be feasible but expensive. Both of these approaches would apply to a particular material for a particular manufacturing process: neither would be capable of providing a generic material model.
The algorithm process of arranging pores within the bulk of material is probably a reasonable approximation to the real emergence of pores within a material; on that basis, the pore placement algorithm could be a reasonable approach. However, close to the material surface, any real pores that form there could actually burst out of the surface and become part of the surface profile. A geometry creation algorithm that reflects real processes better might provide more realistic geometry; for example, a surface formed by pore busting, or a surface formed by the finish machining cutting through a sub-surface pore. The results from these two different model types might help determine how beneficial finish machining is for enhancing life.
The choice of circular pores is a natural and easy one: if a pore arises from trapped gas in a near constant pressure field within a near homogeneous semi-liquid material, then the pore it forms is likely to be near spherical. Whether that is the case in many typical real materials is questionable. Likewise, there are similar questions to be raised about the natural formation of an exposed surface, and how the surface profile is created based on thermal and pressure variation as the solidification takes place. The models also assume that there is no initial internal residual stress. The assumptions made here might be reasonably valid for some forms of Additive Manufacturing with post-manufacture heat treatment.

Many other researchers have focussed on the material grain structure and morphology as the driver for their modelling. The significance of the grain structure is another aspect that should be tested in future models.
The load choice and strain-hardening material model used in the Finite Element Analysis (FEA) described in this paper has been tailored to obtain significant levels of equivalent plastic strain (PEEQ) after only a few loading half cycles. To model fatigue crack initiation and propagation in a way that can be compared with test specimen data, it will be necessary to reduce load levels, analyse much higher numbers of cycles, and introduce a mechanism to represent crack propagation. These are significantly greater analysis challenges.
Finally, it has to be said that the easiest models to create and analyse are 2D models, but the real material is 3D. Creating 3D models presents some very significant challenges: much more complexity in geometry creation and control; significantly greater challenges in FEA mesh building; and, for any reasonably sized model, the computation would require High Performance Computing. For now, the results of the 2D analysis work are sufficient to be indicative and qualitative: they inform us about the effects of geometry. For more conclusive and quantitative results, 3D analysis will become necessary.

7.6 Linking these results to fatigue assessment

This paper has almost completed the full circle of the argument. We have discussed the combined role of surface roughness and sub-surface porosity, and explained how these lead to greater *"penetration"* of equivalent plastic strain into the sub-surface region. However, in the literature review, we discussed the suggestion by Gorelik [60], that some measure of the surface roughness could stand as a proxy for an initial crack length for fatigue life prediction using the DTDA analysis [16].

1. We anticipated that this might provide an approach that could capture the effects of surface-breaking cracks, and other features of AM parts, so as to be able to make reliable life predictions for high duty and safety critical components.
2. A further practical aspect of this to consider the dressing the surfaces of AM components: to provide guidelines on the appropriate depth of surface machining needed to remove imperfections, and thereby extend the component operational life.

The results that have been achieved through modelling indicate that the *"PEEQ penetration"* depth is a suitable and meaningful length measurement that might be taken as (or related to) EIDS when performing a durability analysis. To take this forward, it will be necessary to obtain typical surface profile and sub-surface flaw size data for the specimens used in the tests, for example those referenced in [15, 17-18], and to establish that using this value for EIDS yields conservative lives. If successful the results obtained from the present paper could be scaled to match, to provide a candidate EIDS, and hence establish whether this modelling approach has a useful predictive power.
To answer the second point, it should be remembered that surface machining is in itself a manufacturing process. On the one hand it might remove the top layer of a material, but the new surface will have a new surface profile. Furthermore, the sub-surface under that new surface might also contain defects, which might be pre-existing, or have been developed or modified by the machining process itself. Thus, the new surface and its sub-surface would need to be assessed in the same way as the original surface, and a new EIDS assessment made.

7.7 Linking these results to airworthiness requirements

The computational models developed for this paper and for the previous work on which this has been based [56, 63-64] are scale independent. In other words, the dimensions of features

can all be scaled to a reasonable extent, so long as the macroscopic length scale remains representative of the everyday component size, and that the size of the smallest feature is reasonably larger than the atomic length scale limit. By working initially independently of length scale, we avoid biased thinking. Subsequent to performing the computational modelling and analysis, we have re-scaled the dimensions of the models to align with typical surface roughness size (≤ 0.1 mm) and a maximum defect size (≤ 0.1 mm) that is similar to the EIDS suggested in EZ-SB-19-01. It is these re-scaled values that are presented.

On inspection of Figures 5 and 6, and Table 3, we see the penetration depth of the equivalent plastic strain (PEEQ) into the sub-surface of the component. For this particular data, the surface roughness size is ≤ 0.1 mm, and the maximum defect size (pore diameter) is 0.05 mm. Considering surface roughness alone, the PEEQ penetration is around 0.25 mm; and considering porosity alone, it is around 0.4 mm. For the combined effect of surface roughness and porosity, the PEEQ penetration is around 0.55 mm. Furthermore the material which has undergone plastic strain is networked, meaning that these are not isolated pockets of strain, but paths in the material that represent potential failure.

Remember, that this analysis did not include element deletion or other mechanisms for modelling failure, but bulk materials will generally fail at sufficiently high levels of strain. In these models, we have also demonstrated that the strain pattern is established on the first load application, and that, while repeated load cycles increase the level of strain, there is little further change to the overall pattern of strain. In other words, for two otherwise similar materials, if one exhibits a higher strain to failure characteristic than the other then it will endure more load cycles, but will fail in a similar way. Essentially, this means that we can read across between materials and fatigue test data: it is a possible partial explanation as to why the fatigue test data collected is so consistently mapped across to the Hartman-Schijve variant of the NASGRO equation.

Now let us consider the PEEQ penetration depth. The network pattern shown in Figure 5, and also in Figures 7 and 8 for different maximum pore diameters and porosity distribution, is consistent in form and PEEQ penetration depth. If we compare the penetration depth to the EIDS of 0.01 inches (0.254 mm) suggested in EZ-SB-19-01 [6] we see a similar order of magnitude. Considering the surface roughness alone, then there is a near perfect match; however, it is not conservative to assume that there are no sub-surface defects. Even if our models are not particularly representative, they do indicate an important additional effect. Indeed, for the larger size pores (0.1 mm) and for the higher concentrations (Figure 7(d) and Table 3, 4th row), the PEEQ penetration reaches 0.73 mm. One could say that this suggests the EIDS should be increased to 0.03 inches (0.762 mm), but this would be failing to remember the scaling, and the fact that any EIDS must be determined analytically and must result in a conservative estimate of the operational life of the part. The scaling seems to be more important to the surface roughness, but there remains a difficulty in how to characterize the roughness, since it is the relative distance between neighbouring deeper furrows that seems to be important.

8. CONCLUSIONS

The results from the analyses presented here show that the effect of surface roughness and sub-surface porosity is summative. If either the roughness or the porosity is neglected, then the development over multiple load cycles of equivalent plastic strain in the sub-surface will be under-represented. There is significant coupling between the porosity and the roughness pits, meaning that two pits that are reasonably well-spaced can actually work together in combination with sub-surface porosity to weaken a wedge of material in the sub-surface. This is also suggestive as a mechanism for stress related corrosion.

Greater levels of porosity in the sub-surface imply greater equivalent plastic strain penetration into the bulk material; however, for larger numbers of reasonably homogenously arranged smaller pores the plastic strain creates a network. This seems to be an emergent phenomenon arising from the random distribution.

The results presented here for the larger pore examples are not an ideal fit with the other data generated. This is because of the small numbers of the pores, and the relatively poorly defined domain over which the pores could be defined. The problem could be resolved by increasing the problem size, increasing the number of pores within the model, and having greater control over the porosity distribution.

Each of the models presented shows some similar features. In each case, under first loading, the presence of stress raiser features – surface roughness and porosity – leads to local stresses exceeding the yield stress of the material, and the formation of localised zones of equivalent plastic strain. The shape of each of these zones is similar, but varies in size with the pore size. As the number of load cycles is increased, the area of these zones of plastic strain remains the same, or does not grow significantly, but the level of plastic strain increases within that area. High plastic strain could indicate local failure, so this is suggestive of a failure initiation mechanism.

Overall, the *"PEEQ penetration"* – the greatest depth into the sub-surface where there is plastically strained material – increases with increasing pore size, and reducing spacing between pores. A more significant effect is that the combined effect of porosity and surface roughness is to generate "<" shaped networks of PEEQ into the material, defined on the surface by nearby deeper furrows in the surface. Characterization of the PEEQ penetration would depend most critically on the analysis of the surface roughness data to identify these potentially damaging furrow spacings.

The data presented here is indicative only, and further modelling work will be required to describe the trends with more precision. It is proposed that the *"PEEQ penetration"* depth be used as a proxy for the EIDS to be used in the Hartman-Schijve variant of the NASGRO equation, and life predictions be made on that basis. These computed lives must then be compared with test data, to test whether this can provide a conservative basis for life prediction.

COMPLIANCE WITH ETHICAL STANDARDS:

The authors declare that they have no conflict of interest.

REFERENCES

1. F. Bacon, Novum Organum (1620) available from various sources in the original Latin, and in translations, for example: F. Bacon, Novum Organum, Urbach P (translator), Gibson J (ed), Open Cour Publishing Company, Paul Carus Student Editions, 1994; or F. Bacon Novum Organum, Silverthorne M (translator) Jardine L (introduction), Cambridge Texts in the History of Philosophy, Cambridge University Press, 2008.
2. P. Li, D. H. Warner, A. Fatemi and N. Phan, "Critical assessment of the fatigue performance of additively manufactured Ti–6Al–4V and perspective for future research," *Int J Fatigue,* vol. 85, pp. 130–143, 2016. DOI https://doi.org/10.1016/j.ijfatigue.2015.12.003
3. S. Ford and M. Despeisse, "Additive manufacturing and sustainability: an exploratory study of the advantages and challenges," *Journal of Cleaner Production,* vol. 137, pp. 1573-1587, 2016. DOI https://doi.org/10.1016/j.jclepro.2016.04.150

4. S. K. Everton, M. Hirsch, P. Stravroulakis, R. K. Leach and A. T. Clare, "Review of in-situ process monitoring and in-situ metrology for metal additive manufacturing," *Materials and Design,* vol. 95, pp. 431-445, 2016. https://doi.org/10.1016/j.matdes.2016.01.099
5. MIL-STD-1530D, Department Of Defense Standard Practice: Aircraft Structural Integrity Program (ASIP), 31-Aug-2016.
6. C. A. Babish IV, EZ-SB-19-01, Structures Bulletin AFLCMC/EZ, Bldg. 28, 2145 Monahan Way, WPAFB, OH 45433-7101, 2019.
7. S. Beretta and S. Romano, "A comparison of fatigue strength sensitivity to defects for materials manufactured by AM or traditional processes," *Int J Fatigue,* vol. 94, pp. 178-191, 2017. DOI https://doi.org/10.1016/j.ijfatigue.2016.06.020
8. M. Kahlin, H. Ansell and J.J. Moverare, "Fatigue behaviour of notched additive manufactured Ti6Al4V with as-built surfaces," *Int J Fatigue*, vol. 101, pp. 51–60, 2017. DOI https://doi.org/10.1016/j.ijfatigue.2017.04.009
9. M. Kahlin, H. Ansell and J.J. Moverare, "Fatigue behaviour of additive manufactured Ti6Al4V, with as-built surfaces, exposed to variable amplitude loading," *Int J Fatigue,* vol. 103, pp. 352–363, 2017. DOI https://doi.org/10.1016/j.ijfatigue.2017.06.023
10. D. Greitemeier, C. Dalle Donne, F. Syassen, J. Eufinger and T. Melz, "Effect of surface roughness on fatigue performance of additive manufactured Ti–6Al–4V," *Mat Sci Tech*, vol. 32, pp. 629-634, 2016. DOI https://doi.org/10.1179/1743284715Y.0000000053
11. K. S. Chan "Characterization and analysis of surface notches on Ti-alloy plates fabricated by additive manufacturing techniques," *Surface Topography: Metrology and Properties,* 2015. DOI https://doi.org/10.1088/2051-672X/3/4/044006
12. S. Leuders, M. Vollmer, F. Brenne, T. Troster and T. Niendorf, "Fatigue Strength Prediction for Titanium Alloy TiAl6V4 Manufactured by Selective Laser Melting," *Metall and Mat Trans A*, vol. 46, pp. 3816–3823, 2015. DOI https://doi.org/10.1007/s11661-015-2864-x
13. H. Masuo, Y. Tanaka, S. Morokoshi, H. Yagura, T. Uchida, Y. Yamamoto and Y. Murakami, "Influence of defects, surface roughness and HIP on the fatigue strength of Ti-6Al-4V manufactured by additive manufacturing," *Int J Fatigue,* vol. 117, pp. 163-179, 2018. DOI https://doi.org/10.1016/j.ijfatigue.2018.07.020
14. K. S. Chan and A. Peralta-Duran, "A Methodology for Predicting Surface Crack Nucleation in Additively Manufactured Metallic Components," *Metallurgical and Materials Transactions A,* vol. 50A, pp. 4378-4387, 2019. DOI https://doi.org/10.1007/s11661-019-05309-7
15. R. Jones, R. K. Singh Raman and A. J. McMillan, "Crack growth: Does microstructure play a role?" *Eng Frac Mech*, vol. 187, pp. 190-210, 2018. DOI https://doi.org/10.1016/j.engfracmech.2017.11.023
16. R. Jones "Fatigue crack growth and damage tolerance," *Fatigue Fract Eng Mater Struct,* vol. 37, pp. 463-83, 2014. DOI https://doi.org/10.1111/ffe.12155
17. K. Ali, D. Peng, R. Jones, R. K. Singh Raman, X. L. Zhao, A. J. McMillan and F. Berto, "Crack growth in a naturally corroded bridge steel," *Fatigue Fract Eng Mater Struct*, vol. 40, pp. 1117-1127, 2017. DOI https://doi.org/10.1111/ffe.12568

18. R. Jones, P. Huang and D. Peng, "Crack growth from naturally occurring material discontinuities under constant amplitude and operational loads," *Int J Fatigue*, vol. 91, pp. 434-44, 2016. DOI https://doi.org/10.1016/j.ijfatigue.2016.02.010

19. S. C. Forth, The purpose of generating fatigue crack growth threshold data, NASA Johnson Space Center, 2006. http://ntrs.nasa.gov/

20. K. Wang, F. Wang, W. Cui, T. Hayat and B. Ahmad, "Prediction of short fatigue crack growth of Ti-6Al-4V," *Fatigue Fract Eng Mater Struct,* vol. 37, pp. 1075-86, 2014. DOI https://doi.org/10.1111/ffe.12177

21. Y. Zhai, H. Galarraga and D. A. Lados, "Microstructure, static properties, and fatigue crack growth mechanisms in Ti-6Al-4V fabricated by additive manufacturing: LENS and EBM," *Eng Fail Analysis*, vol. 69, pp. 3-14, 2016. DOI https://doi.org/10.1016/j.engfailanal.2016.05.036

22. D. Peng, P. Huang and R. Jones, "Practical computational fracture mechanics for aircraft structural integrity," In: Jones R, Baker A, Matthews N, Champagne V (eds), Aircraft Sustainment and Repair, Butterworth-Heinemann Press, Oxford, pp. 67-128, 2018.

23. R. Jones, J. G. Michopoulos, A. P. Iliopoulos, R. K. Singh Raman, N. Phan and T. Nguyen, "Representing Crack Growth In Additively Manufactured TI-6AL-4V," *Int J Fatigue,* vol. 116, pp. 610-622, 2018. DOI https://doi.org/10.1016/j.ijfatigue.2018.07.019

24. A. P. Iliopoulos, R. Jones, J. G. Michopoulos, N. Phan and R. K. Singh Raman, "Crack growth in a range of additively manufactured aerospace structural materials," *Aerospace*, 2018. https://doi.org/10.3390/aerospace5040118

25. R. Jones, N. Matthews, D. Peng, N. Phan, and T. T. Nguyen, "Damage Tolerant Assessment Of Additively Manufactured Replacement Parts," Proc. 13th Int Conf Mechanical Behaviour of Materials (ICM13), Melbourne, Australia, 11 -14 June 2019.

26. R. Jones, N. Matthews, D. Peng, N. Phan and T. Nguyen, "Applications of SPD to enhance the structural integrity of corroded airframes," In: Jones R, Baker A, Matthews N, Champagne V (eds), Aircraft Sustainment and Repair, Butterworth-Heinemann Press, Oxford, pp. 863-906, 2018.

27. N. Matthews, L. Molent, S. Barter and R. Jones, "Application of SPD to enhance the structural integrity of fuselage skins and centre barrels," In: Jones R, Baker A, Matthews N, Champagne V (eds), Aircraft Sustainment and Repair, Butterworth-Heinemann Press, Oxford, pp. 907-930, 2018.

28. EZ-SB-13-001 Structures Bulletin, AFLCMC/EZ, Bldg. 28, 2145 Monahan Way, WPAFB, OH 45433-7101, 2013.

29. J. Lincoln and R. A. Melliere, "Economic Life Determination for a Military Aircraft," *AIAA Journal of Aircraft*, vol. 36, pp. 737-742, 1999. https://doi.org/10.2514/2.2512

30. M. Lo, R. Jones, A. Bowler, M. Dorman and D. Edwards, "Crack growth at fastener holes containing intergranular cracking," *Fatigue Fract Eng Mater Struct,* vol. 40, pp. 1664–1675, 2017. DOI https://doi.org/10.1111/ffe.12597

31. D. Tamboli, S. Barter and R. Jones, "On the growth of cracks from etch pits and the scatter associated with them under a miniTWIST spectrum," *Int J Fatigue,* vol. 109, pp. 10-16, 2018. DOI https://doi.org/10.1016/j.ijfatigue.2017.12.002

32. R. Jones, D. Peng and A. J. McMillan, "Crack growth from naturally occurring material discontinuities," In: Jones R, Baker A, Matthews N, Champagne V (eds), Aircraft Sustainment and Repair, Butterworth-Heinemann Press, Oxford, pp. 129-190, 2018.

33. T. Yuri, Y. Ono and T. Ogata, "Effects of surface roughness and notch on fatigue properties for Ti–5Al–2.5Sn ELI alloy at cryogenic temperatures," *Science and Technology of Advanced Materials,* vol. 4, pp. 291-299, 2003. DOI https://doi.org/10.1016/S1468-6996(03)00058-5

34. J. Lai, H. Huang and W. Buising, "Effects of microstructure and surface roughness on the fatigue strength of high-strength steels," *Procedia Structural Integrity,* vol. 2, pp. 1213-1220, 2016. DOI https://doi.org/10.1016/j.prostr.2016.06.155

35. A. Townsend, N. Senin, L. Blunt, R. K. Leach and J. S. Taylor, "Surface texture metrology for metal additive manufacturing: a review," *Precision Engineering,* vol. 46, pp. 34-47, 2016. DOI https://doi.org/10.1016/j.precisioneng.2016.06.001

36. A. Triantaphyllou, C. L. Giusca, G. D. Macaulay, F. Roerig, M. Hoebel, R. K. Leach, B. Tomita and K. A. Milne, "Surface texture measurement for additive manufacturing," *Surf Topogr: Metrol Prop*, 2015. DOI https://doi.org/10.1088/2051-672X/3/2/024002

37. B. B. Mandelbrot, D. E. Passoja and A. J. Paullay, "Fractal character of fracture surfaces of metals," *Nature*, vol. 308, pp. 721–722, 1984. DOI https://doi.org/10.1038/308721a0

38. B. B. Mandelbrot, "Fractal analysis and synthesis of fracture surface roughness and related forms of complexity and disorder," *Int J Fracture,* vol. 138, pp. 13–17, 2006. DOI https://doi.org/10.1007/s10704-006-0037-z

39. E. Bouchaud, "Scaling properties of cracks," *J Phys: Condens Matter*, vol. 9, pp. 4319–4344, 1997. DOI https://doi.org/10.1088/0953-8984/9/21/002

40. R. Jones, N. Matthews, C. A. Rodopoulos, K. Cairns and S. Pitt, "On the use of supersonic particle deposition to restore the structural integrity of damaged aircraft structures," *Int J Fatigue,* vol. 33, pp. 1257-1267, 2011. DOI https://doi.org/10.1016/j.ijfatigue.2011.03.013

41. R. Jones, F. Chen, S. Pitt, M. Paggi and A. Carpinteri, "From NASGRO to fractals: Representing crack growth in metals," *Int J Fatigue,* vol. 82, pp. 540-549, 2016. DOI https://doi.org/10.1016/j.ijfatigue.2015.09.009

42. J. Liu, M. K. Chaudhury, D. H. Berry, J. E. Seebergh, J. H. Osborne and K. Y. Blohowiak, "Effect of Surface Morphology on Crack Growth at a Sol-Gel Reinforced Epoxy/Aluminum Interface," *The Journal of Adhesion*, vol. 82, pp. 487–516, 2006. DOI https://doi.org/10.1080/00218460600713725

43. C. B. Finfrock, A. Exil, J. D. Carroll and L. Deibler, "Effect of Hot Isostatic Pressing and Powder Feedstock on Porosity, Microstructure, and Mechanical Properties of Selective Laser Melted AlSi10Mg," *Metallography, Microstructure, and Analysis*, vol. 7, pp. 443-456, 2018. DOI https://doi.org/10.1007/s13632-018-0456-z

44. A. du Plessis, S. G. le Roux, J. Els, G. Booysen and D. C. Blaine, "Application of micro CT to the non-destructive testing of an additive manufactured titanium component," *Case Studies in Nondestructive Testing and Evaluation,* vol. 4, pp. 1–7, 2015. DOI http://dx.doi.org/10.1016/j.csndt.2015.09.001

45. S. Tammas-Williams, H. Zhao, F. Léonard, F. Derguti, I. Todd and P. B. Prangnell, "XCT analysis of the influence of melt strategies on defect population in Ti–6Al–4V

components manufactured by Selective Electron Beam Melting," *Materials Characterization,* vol. 102, pp. 47-61, 2015. DOI http://dx.doi.org/10.1016/j.matchar.2015.02.008

46. F. Léonard, S. Tammas-Williams, P. B. Prangnell, I. Todd and P. J. Withers, "Assessment by X-ray CT of the effects of geometry and build direction on defects in titanium ALM parts," Conf. Industrial Computed Tomograpy (iCT) (Wels: Austria: Shaker Verlag) 85-93, 2015.
47. W. Guo, R. Sun, B. Song, Y. Zhu, F. Li, Z. Che, B. Li, C. Guo, L. Liu and P. Peng, "Laser shock peening of laser additive manufactured Ti6Al4V titanium alloy," *Surface & Coatings Technology,* vol. 349, pp. 503-510, 2018. DOI https://doi.org/10.1016/j.surfcoat.2018.06.020
48. J. P. Kruth, G. Levy, F. Klocke and T. H. C. Childs, "Consolidation phenomena in laser and powder-bed based layered manufacturing," *Annals of the CIRP* vol. 56/2/2007, pp. 730-759, 2007. DOI https://doi.org/10.1016/j.cirp.2007.10.004
49. J. Mardaras, P. Emile and A. Santgerma, "Airbus approach for F&DT stress justification of Additive Manufacturing parts," *Procedia Structural Integrity,* vol. 7, pp. 109–115, 2017. DOI https://doi.org/10.1016/j.prostr.2017.11.067
50. D. Jeulin, W. Li and M. Ostoja-Starzewski, "On the geodesic property of strain field patterns in elastoplastic composites," *Proc. R. Soc. A*, vol. 464, pp. 1217-1227, 2008. DOI https://doi.org/10.1098/rspa.2007.0192
51. S. Li, "General unit cells for micromechanical analyses of unidirectional composites," *Composites: Part A*, vol. 32, pp. 815-826, 2001. DOI https://doi.org/10.1016/S1359-835X(00)00182-2
52. S. Li, "Boundary conditions for unit cells from periodic microstructures and their implications," *Composites Science and Technology*, vol. 68, pp. 1962-1974, 2008. DOI https://doi.org/10.1016/j.compscitech.2007.03.035
53. C. A. Rodopoulos and G. Chliveros, "Fatigue damage in polycrystals – Part 1: The numbers two and three," *Theoretical and Applied Fracture Mechanics,* vol. 49, pp. 61-76, 2008. DOI https://doi.org/10.1016/j.tafmec.2007.10.007
54. C. A. Rodopoulos and G. Chliveros, "Fatigue damage in polycrystals – Part 2: Intrinsic scatter of fatigue life," *Theoretical and Applied Fracture Mechanics,* vol. 49, pp. 77-97, 2008. DOI https://doi.org/10.1016/j.tafmec.2007.10.001
55. A. Brückner-Foit and X. Huang, "Numerical simulation of micro-crack initiation of martensitic steel under fatigue loading," *Int J Fatigue.* Vol. 28, pp. 963-971, 2006. DOI https://doi.org/10.1016/j.ijfatigue.2005.08.011
56. A. J. McMillan, "Material strength knock-down resulting from multiple randomly positioned voids," *J Rein Plastics Composites,* vol. 31, pp. 13-28, 2012. DOI https://doi.org/10.1177/0731684411422614
57. A. J. McMillan, "Defect identification and characterization algorithms for assessing effect on component strength," Proc 15th European Conf. Composite Materials, Venice, Italy, 24-28 June 2012.
58. A. J. McMillan, "Geometry generation challenges for modelling and analysis of micro-structured materials," *IOP Conf Ser: Mater Sci Eng,* 2015. DOI https://doi.org/10.1088/1757-899X/74/1/012010

59. W. D. Pilkey and D. F. Pilkey, Peterson's Stress Concentration Factors, 3rd Ed, John Wiley & Sons, Hoboken, New Jersey, 2008.

60. M, Gorelik, "Additive manufacturing in the context of structural integrity," *Int J Fatigue*. Vol. 94, pp. 168–77, 2017. DOI https://doi.org/10.1016/j.ijfatigue.2016.07.005

61. M. A. Wiśniewska, "The ISO 25178 standards for areal surface texture measurements: a critical appraisal," In Gajadhur M, Markowski K, Badyda AJ (Eds) The challenges of contemporary science: Theory and applications, Fundacja na rzecz młodych naukowców, pp. 165-166, 2014.

62. M. Bramowicz, S. Kulesza, T. Lipiński, P. Szabracki and P. Piatkowski, "Fractal Analysis of AFM Data Characterizing Strongly Isotropic and Anisotropic Surface Topography," *Solid State Phenomena,* vol. 203-204, pp. 86-89, 2013. DOI https://doi.org/10.4028/www.scientific.net/SSP.203-204.86

63. A. McMillan, R. Jones, D. Peng, G. A. Chechkin, "A computational study of the influence of surface roughness on material strength," *Meccanica,* vol. 53, pp. 2411-2436, 2018. DOI https://doi.org/10.1007/s11012-018-0830-6

64. A. J. McMillan, D. Peng, R. Jones, N. Pham and J. G. Michopoulos, "Additive manufacturing: implication of surface finish on component life," Proc. SAMPE Europe Conference, Southampton, UK, 11-13 September 2018.

65. P. A. Kobryn and S. L. Semiatin, "The laser additive manufacture of Ti-6Al-4V," *JOM,* vol. 53, pp. 40-2, 2001. DOI https://doi.org/10.1007/s11837-001-0068-x

66. R. Jones, L. Molent and S. Barter, "Calculating crack growth from small discontinuities in 7050-T7451 under combat aircraft spectra," *Int J Fatigue,* vol. 55, pp. 178-82, 2013. DOI https://doi.org/10.1016/j.ijfatigue.2013.06.009

67. R. Jones, R. K. Singh Raman, A. P. Iliopoulos, J. G. Michopoulos, N. Phan and D. Peng, "Additively manufactured Ti-6Al-4V replacement parts for military aircraft," *Int J Fatigue,* vol. 124, pp. 227-235, 2019. DOI https://doi.org/10.1016/j.ijfatigue.2019.02.041

68. ASTM, Measurement of Fatigue Crack Growth Rates, ASTM E647-13, USA, 2013.

69. Abaqus Manuals, Dassault Systèmes Simulia Corporation, Providence.

70. The Python Software Foundation, https://www.python.org/

71. A. J. C. B. Saint-Venant, "Memoire sur la Torsion des Prismes," *Mem Divers Savants,* vol. 14, pp. 233–560, 1855.